ELECTRON NUCLEAR DOUBLE RESONANCE (ENDOR) STUDIES

of $^{53}Cr^{3+}$ IN ALUMINUM ALUMS

by

Brian Auger

Submitted in partial fulfillment
of the requirements for the degree of
Master of Science

Department of Physics
Faculty of Science and Engineering
University of Ottawa
Ottawa, Canada

1974

Acknowledgments

The author wishes to thank Dr. Armen Manoogian for his suggestion of the research problem, for his useful collaboration and guidance and his patience during the course of this work.
Mr. Bei Wah Chan also deserves thanks for his part in the operation of the spectrometers. Financial assistance from Dr. Manoogian's National Research Council Grant is gratefully acknowledged. Thanks are also due to Mrs. L. Leroux for her speedy and accurate typing of the thesis.

Abstract

The techniques of electron spin resonance (ESR) and electron nuclear double resonance (ENDOR) were used to study the energy level splittings of $^{53}Cr^{3+}$ impurities in $RbAl(SO_4)_2 \cdot 12H_2O$ and $CsAl(SO_4)_2 \cdot 12H_2O$ alums. ESR measurements were made at room, liquid nitrogen and liquid helium temperatures, while ENDOR measurements were made at liquid helium temperature. All work was done at X-band microwave frequencies ($\nu \sim 9.4$GHz). The ESR study allowed the spin Hamiltonian D parameter and g-values to be determined. Values of the spin Hamiltonian hyperfine parameters A, B, Q' and g_n' were determined from the ENDOR work and compared with values obtained by others in the corresponding gallium alums and in guanidine aluminum sulfate hexahydrate (GAlSH). In all the above mentioned crystals the chromium impurity ion is surrounded by an octahedron of six water molecules which has a small trigonal distortion superimposed. The reason for the trigonal distortion and its relation to the D parameter has been the subject of much discussion. Since the Q' parameter and the quantity A-B both give a measure of the distortion, a plot of (A-B) vs Q' is given. The plot indicates that the amount of distortion at the chromium site can be related to the type of monovalent ion present (i.e. Rb or Cs) in the alums studied. Furthermore, nearly linear relationships appear to exist between Q' vs D, (A-B) vs D and V_{zz} vs D for all the ENDOR data obtained so far in the alums and in GAlSH. These

relationships may be generally true for trigonally distorted $Cr^{3+}.6H_2O$ complexes in crystals with D-values not too close to zero.

Table of Contents

List of Figures

List of Tables

CHAPTER I

INTRODUCTION

Electron nuclear double resonance (ENDOR) is a powerful tool for investigating the immediate surroundings of a centre with unpaired electrons in a solid. Using the high precision of the ENDOR technique, which is about a thousand times greater than that of ordinary electron spin resonance (ESR), direct measurements of the hyperfine energy level splittings of the paramagnetic centre can be made and precise values of the spin Hamiltonian hyperfine parameters can be calculated. By considering the magnitudes and signs of the various parameters found, in comparison with the values obtained by others in different crystal systems, one is able to make deductions regarding the behaviour of the crystals and to interpret, evaluate and extend the existing theories.

The present study was undertaken to corroborate, if possible, and extend the work described by Danilov[1] who, working with $^{53}Cr^{3+}$ in rubidium gallium and caesium gallium alums, reported the first ENDOR work on the alums as well as the first ENDOR studies of the $^{53}Cr^{3+}$ ion centres in a trigonally distorted octahedron of water molecules. In the above studies several hypotheses were postulated regarding the relationships between the spin Hamiltonian parameters

and the behavior of the crystal. These hypotheses are supported and several new relationship are suggested by the present work, which involves $^{53}Cr^{3+}$ in rubidium aluminum and caesium aluminum alums.

CHAPTER II

CRYSTALLOGRAPHY

II 1 Introduction

The alums are a group of double salts having the general formula:

$$M^{+1}M^{+3}(M^{+6}O_4)_2 \cdot 12H_2O \ ,$$

where M^{+1} is a monovalent metal ion, M^{+3} is a trivalent metal ion and M^{+6} is a sulfur, selenium or tellurium ion. The unit cell, whose lattice parameter is approximately 12 $\mathring{A}$, contains four formula units. In the work described, M^{+1} is caesium or rubidium, M^{+3} is aluminum and M^{+6} is sulfur. The alum crystals were grown from an aequeous solution of the constituent sulfates in stochiometric proportion plus a small amount of chromium sulfate dopant. The chromium entered the aluminum site at dopant levels of approximately 0.01% by weight of aluminum.

II 2 Investigation of Alum Structure - Historical.

The first X-ray work on the alums was published by Vegard and Schjelderup[2] in 1917 but the lack of sophistication in the equipment led to an incorrect assignment of the space group. The space group was correctly identified as Pa3 by Wyckoff[3] in 1923. Further

improvement was made by Lipson and Beevers [4] (1934) and Lipson [5] (1935), the latter author grouping the alums into three types termed α, β and γ. The type of alum formed was said to depend on the size of the monovalent cation as follows:

α .....intermediate (eg. Rb)

β .....large (eg. Cs)

γ .....small (only one known example, Na)

In 1965 and 1966, Cromer, Kay and Larsen [6], using X-ray and neutron diffraction techniques, refined the structures of certain alums, including CsAl alum and RbAl alum. These studies revealed more precisely the positions and bond angles of the various atoms in these alums but did not alter the previous system of classification of the alums.

II 3 The Waters

In the alums there are two crystallographically different groups of six water molecules: those associated with the monovalent cation and those associated with the trivalent cation. The waters around the trivalent ion form a nearly regular octahedron. The orientation of the octahedron with respect to the cell axes is different in each of the three types as follows.

II 3(i) α-type: In the α-type alums the [111] axis of the octahedron coincides with [111] axis of the crystal, but the cubic axes of the

octahedron are displaced from the crystal axes by a rotation of about 9.5^{o} about the [111] direction. The octahedron has a small trigonal distortion along the crystal [111] direction.

II 3(ii) β-type: The β type alums have perfectly regular groups of water molecules. The axes of the octahedron are directed along the crystal cubic axes. The trigonal distortion is also present in the β-type.

II 3(iii) γ-type: In the γ-type alums the water molecules about the trivalent cation form a perfect octahedron which is rotated by 39.4^{o} about the threefold axis.

II 3(iv) The waters around the monovalent ion form a highly distorted octahedron. In the β alums the water octahedron is compressed along the threefold axis and stretched out normal to this axis until it is nearly planar. The two ends of the resulting trigonal antiprism are separated by only about 0.06 Å. The α alums are also characterized by this compression although it is less pronounced. In the γ alum the octahedron of waters about the sodium atom is somewhat distorted by being stretched out along the threefold axis of the cell.

II 4 The Sulfate Groups

II 4(i) β-type: In the β-alums the sulfate group forms an almost perfect tetrahedron. The sulfur ion and one of the oxygens is situated on the [111] crystal axis and they are oriented in such a way that the three other oxygens fit into the spaces around the monovalent cation made by the distorted trigonal antiprism of waters.

This occurs on both sides of the monovalent cation. The six sulfate oxygen atoms are about the same distance from the cation as are the water molecules. Hence, a slightly distorted cubic-close packed array of oxygen atoms surrounds the cation, giving it a twelve-fold coordination.

II 4(ii) γ-type: The angles in the sulfate group in the γ alums depart from those of a regular tetrahedron by a small but significant amount. Also, the sulfate group has an orientation opposite to that of the β alums.

II 4(iii) α-type: The α alums are disordered in terms of the orientation of the sulfate groups; that is some sulfate groups are oriented as in β and some as in the γ alums. The fraction of reversed sulfate groups tends to increase as the monovalent cation becomes smaller.

II 5 Space Group Assignment

As previously noted the space group of the alums is Pa3. The 'P' indicates that the unit cell is "primitive". That is, its basic structure comprises one atom in each corner of a cubic cell. The 'a' designates a set of glide planes which perform a mirror reflection and then a glide 1/2 the unit cell length to all atoms in the cell. The '3', the characteristic of the cubic system, represents a set of four inclined threefold axes in the <111> directions.

CHAPTER III

THEORY

III 1 Introduction

The interactions which determine the energy levels of the paramagnetic ion and the mathematical form of these interactions are now discussed. The full spin Hamiltonian is explained and the dynamics of the ESR and ENDOR transitions is discussed.

III 2 The Ground State and the Spin Hamiltonian

As a result of the crystal field interaction of the paramagnetic ion with the neighbouring diamagnetic ions in a crystal, the ground state of the paramagnetic ion consists of a group of electronic levels which normally lie at least 10^5 cm^{-1} below all other electronic levels. Because of this large energy gap the lower group can be treated theoretically as being separate from the rest. The behaviour of this group is then represented by defining an effective spin, S, such that the total number of levels in the group is $2S + 1$, the same as in an ordinary spin multiplet. These levels, which are themselves split by interactions with the nucleus, can be thought of as the eigenvalues of an Hamiltonian operator which represents the total electronic energy of the group.

The transitions which occur between these levels produce a

paramagnetic resonance spectrum which is in general very complex. It can be interpreted with the use of a "spin Hamiltonian", a method introduced by Pryce[7] and Abragam and Pryce[8]. Its form can be determined from considerations of crystal symmetry and the interactions which are present. Using this 'spin Hamiltonian', a complete description of the experimental results can be presented by finding the size of the coefficients of a relatively few terms together with the directions of the appropriate interaction axes relative to the crystal axes if anisotropy is present.

III 3 The Crystal Field

In studying dilutely doped samples, such as the crystals grown for this experiment, the following simplifying assumptions are made. First, the influence of the environment on the electronic wave function of the ion can be described by means of a static crystal field. Second, if the paramagnetic ion has the same charge as the diamagnetic ion which it has replaced, so that no charge compensation is required, the symmetry, if not the magnitude of the crystal field it "sees", is unchanged.

Using Hund's rules we calculate that the ground state of a free Cr^{3+} ion is characterized by

$J = 3/2$ where J is the total quantum number

$S = 3/2$ where S is the spin quantum number

$L = 3$ where L is the orbital quantum number

$m = 4$ where m is the multiplicity of the state $\equiv 2S + 1$

In spectroscopic notation this state is written as $^4F_{3/2}$. The initial degeneracy of the state is $(2S + 1)(2L + 1) = 28$. Placing the ion in a cubic crystal electric field lifts some of the orbital degeneracy and reduces the ground state in energy and degeneracy making it a $^4S_{3/2}$ state with a degeneracy of 4.

A small trigonal distortion of the cubic field further splits the exited orbitally degenerate states but no effect is expected on the ground state because it is an orbital singlet. However, matrix elements exist between the ground state and the first exited doublet and singlet for the spin-orbit interaction. Through this indirect mechanism the ground state is resolved into two Kramers' doublets. Kramers has found that an electric field cannot remove any further degeneracy if the ion has an odd number of unpaired electrons, as is the case in Cr^{3+} with three electrons in the d-subshell. The degeneracy is lifted, however, by a magnetic field. The nuclear spin (hyperfine interaction) causes a further splitting of the ground state electronic levels giving rise to hyperfine structure. These levels are shown in figures 1, 2 and 3.

The anisotropic part of the crystal electric field interaction,

Figure 1: The splitting of the $^4F_{3/2}$ state of $^{53}Cr^{3+}$ by the cubic and trigonal components of the crystal field.

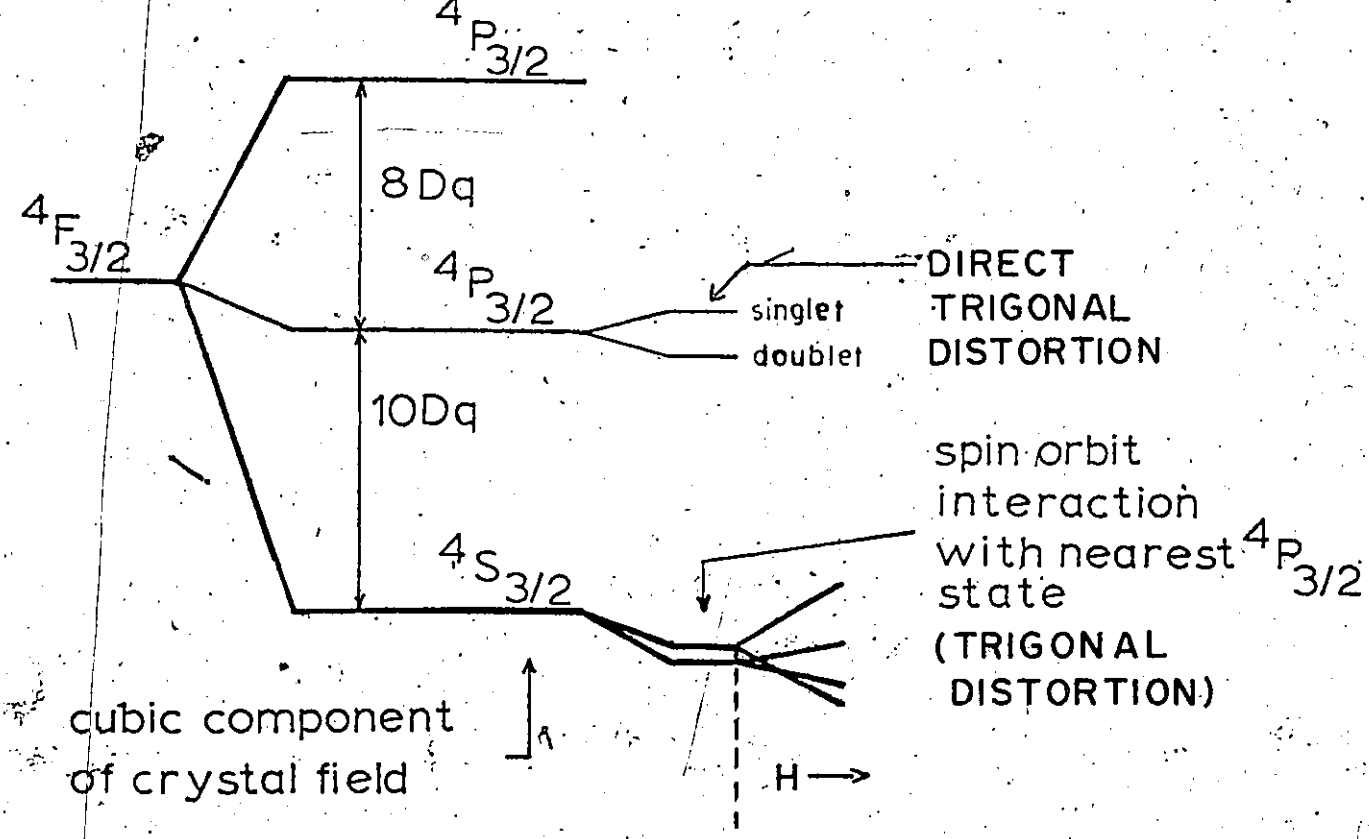
$^4P_{3/2}$
8Dq
$^4F_{3/2}$
$^4P_{3/2}$
singlet
doublet
DIRECT TRIGONAL DISTORTION
10Dq
spin orbit interaction with nearest $^4P_{3/2}$ state
$^4S_{3/2}$
(TRIGONAL DISTORTION)
cubic component of crystal field
H

Figure 2: Energy level diagram of $^{53}Cr^{3+}$ in RbAℓ alum at $4.2^{o}K$ for the z and perpendicular directions.

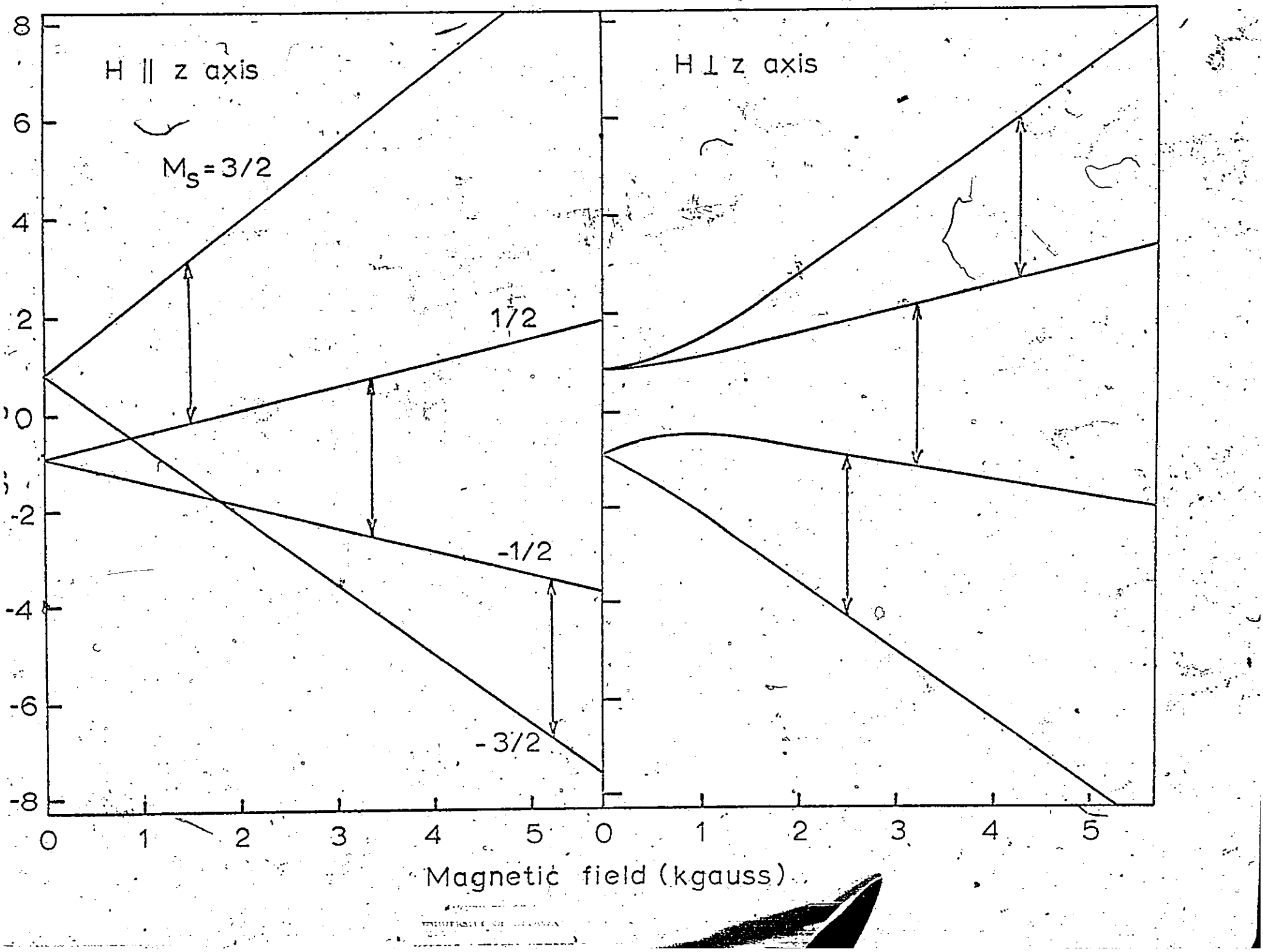
H || z axis
H ⊥ z axis
$M_S = 3/2$
1/2
-1/2
-3/2
8
6
4
2
0
-2
-4
-6
-8
0
1
2
3
4
5
Magnetic field (kgauss)

Figure 3: Hyperfine splitting of $M_s = 3/2$ and $\frac{1}{2}$ levels, for $^{53}Cr^{3+}$. The scale is exagerated, ν_1 is actually $\sim 100\ \nu_2$. The diagram shows the ENDOR process.

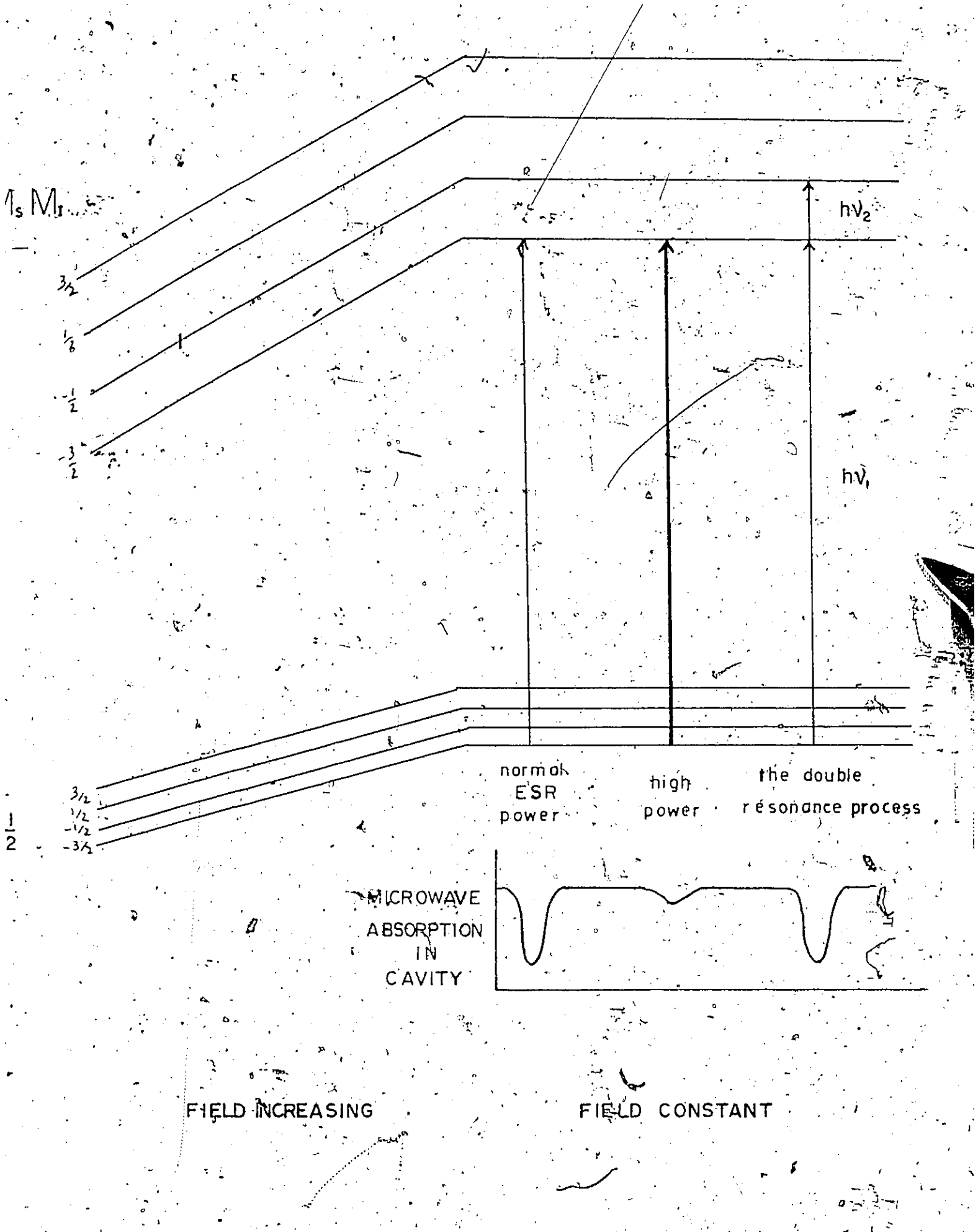
m_s M_I
3/2
1/2
-1/2
-3/2
$h\nu_2$
$h\nu_1$
normal ESR power
high power
the double resonance process
3/2
1/2
-1/2
-3/2
MICROWAVE ABSORPTION IN CAVITY
FIELD INCREASING
FIELD CONSTANT

sometimes called the electronic quadrupole interaction can be expressed as:

$$\vec{S} \cdot \tilde{D} \cdot \vec{S} \qquad (1)$$

where $\vec{S}$ is the spin operator of the ion and $\tilde{D}$ is a tensor quantity. Referred to the principal axes this term is:

$$D_x S_x^2 + D_y S_y^2 + D_z S_z^2 \qquad (2)$$

(N.B.: in the following discussion all tensor quantities are assumed to share the same principal axes).

This can be written:

$$D\{S_z^2 - \tfrac{1}{3}S(S+1)\} + E(S_x^2 - S_y^2) \qquad (3)$$

where

$D = 3/2\ D_z$ is the axial field term.

$E = 1/2(D_x - D_y)$ is the orthorhombic field term.

The crystals studied had an axially symmetric crystal electric field, and so $E = 0$ in this case. The resulting contribution to the spin Hamiltonian is thus:

$$D\{S_z^2 - \tfrac{1}{3}S(S+1)\} \qquad (4)$$

The order of magnitude of the D parameter is 10^{-1} cm^{-1} for Cr^{3+} in the alums.

The D parameter has been expressed theoretically[9] in the following form:

$$D = \tfrac{3}{7}(\lambda/\Delta E)^2 \langle r^2 \rangle V_{zz} \qquad (5)$$

where

λ is the spin-orbit coupling constant of Cr in the crystal.

ΔE is the energy separation between the ground and first exited state.

$\langle r^2 \rangle$ is the average value of r^2 for the Cr^{3+} 3d wave function

V_{zz} is the electric field gradient due to charges and dipoles external to the Cr ion ($= \partial^2 V/\partial z^2$).

III 4 The Hyperfine Interactions

If the nucleus of the paramagnetic ion has a non-zero spin a coupling will exist between the electrons and the nucleus. The coupling can be represented by an interaction between the effective spin of the electrons and the actual spin of the nucleus. This coupling splits each electronic level into $2I + 1$ components which in our case is four. An interaction can also occur between the electrons of the paramagnetic ion and the nuclei of neighbouring atoms which possess a nuclear spin. The study of this phenomenon is called 'distant ENDOR' and will not be discussed here. The presence of the hyperfine interactions is necessary for the application of the ENDOR technique.

III 4(i) The 'A' or hyperfine term: There are two different effects which contribute to this term as indicated in the following equation

$$g g_n \beta \beta_n \vec{I} \cdot \{ \underbrace{\frac{\vec{L}}{r^3} - \frac{\vec{S}}{r^3} + \frac{3\vec{r}(\vec{S}\cdot\vec{r})}{r^5}}_{1} + \underbrace{\frac{8\pi}{3}\delta(\vec{r})\vec{S}}_{2} \qquad (6)$$

where

g is the electronic g-value

g_n is the nuclear g-value

β is the Bohr magneton

β_n is the nuclear magneton

$\vec{L}$ is the orbital angular momentum of the electrons

$\vec{S}$ is the spin angular momentum of the electrons

$\delta(r)$ is the Dirac-Delta function

First, there is the dipolar interaction between the magnetic moments due to the nuclear and electronic spin. Second, there is the Fermi contact term which is proportional to the unpaired spin density at the nucleus. This quantity is zero for all orbitals except the s-type and so is expected to be zero for our case since the chromium d-orbitals have a zero spin density at the nucleus. It is found, however, that the measured hyperfine splittings exceed considerably the value predicted by the dipole-dipole interaction. Moser[10] has found that core polarization, the effect on the s-electrons of the unpaired d-electrons, is probably responsible for this.

This term can be written in the spin Hamiltonian formalism as

$$\vec{S} \cdot \tilde{A} \cdot \vec{I} \qquad (7)$$

When referred to its principal axes this term takes the form

$$A_x S_x I_x + A_y S_y I_y + A_z S_z I_z \qquad (8)$$

When axial symmetry is present we may use the form

$$A_{\perp}(S_xI_x + S_yI_y) + A_{\parallel}S_zI_z \qquad (9)$$

In the literature, $A_{\parallel}$ is usually referred to as A and $A_{\perp}$ as B. This interaction appears in the Hamiltonian as

$$AS_zI_z + B(S_xI_x + S_yI_y) \qquad (10)$$

The order of magnitude of the A and B terms is $\sim 10^{-3}cm^{-1}$ for $^{53}Cr^{3+}$.

III 3(ii) The Quadrupole Term: When the nucleus has a spin $I > 1$ and there is also an electric field gradient at the nucleus, an interaction with the nuclear quadrupole moment may arise. This results in small changes in the energy levels as determined by the A interaction. The nuclear quadrupole moment is defined by

$$Q = \frac{1}{e}\int \rho r^2(3\cos^2\theta - 1)dV \qquad (11)$$

where

ρ is the nuclear charge density

r is the distance from the centre of gravity of the nuclear charge to the volume element dV

θ is the angle between r and the spin axes z.

e is the proton charge

If the charge distribution is in the shape of a prolate spheroid, using the spin axis as a reference, Q is positive. If the charge distribution has the shape of an oblate spheroid, Q is negative. The nuclear quadrupole interaction constant Q', used in the spin Hamiltonian can be written in terms of the quadrupole moment of ^{53}Cr

as

$$Q' = \frac{3eQV_{zz}}{4I(2I - 1)} (1 - \gamma_\infty) \qquad (12)$$

where $(1 - \gamma_\infty)$ is the Sternheimer antishielding factor for $^{53}Cr^{3+}$ $(= 12.0 \pm 1.0)$.

In the formalism of the spin Hamiltonian this interaction is written as

$$\vec{I} \cdot \tilde{Q}' \cdot \vec{I} \qquad (13)$$

which, referred to its principal axes, becomes

$$Q'_x I_x^2 + Q'_y I_y^2 + Q'_z I_z^2 \qquad (14)$$

This is similar in form to the D tensor.

Thus, by analogy, we can write

$$Q'_{||}\{ [I_z^2 - \tfrac{1}{3}I(I + 1)] + \tfrac{1}{3}\eta(I_x^2 - I_y^2)\} \qquad (15)$$

where

$$Q'_{||} = \tfrac{3}{2}Q'_z \quad \text{and} \quad \eta = \frac{(Q'_x - Q'_y)}{Q'_z}$$

which simplifies in the case of axial symmetry to

$$Q'_{||}\{I_z^2 - \tfrac{1}{3} I (I + 1)\} \qquad (16)$$

and which we will write as

$$Q' \{I_z^2 - \tfrac{1}{3} I(I + 1)\} \qquad (17)$$

The order of magnitude of Q' is $\sim 10^{-5} cm^{-1}$ for $^{53}Cr^{3+}$ in alums.

III 3(iii) The Nuclear Zeeman Interaction: A second small change in the energy of the hyperfine levels is caused by the interaction between the nuclear magnetic moment and the external magnetic field. When an external magnetic field is applied, the electronic wavefunction is changed by an amount that is in the first approximation proportional to H and the electronic magnetic field at the nucleus is modified producing a sort of paramagnetic shielding (or anti-shielding). Consequently the interaction parameter g_n' is not simply a scalar quantity equal to the nuclear g-factor. In fact, in a solid this effect can be large enough that the (anti-)shielding correction may outweigh the direct interaction. When the electronic ground state is anisotropic the (anti-)shielding will be anisotropic so that g_n' becomes a tensor, usually with the same principal axes as the electronic g-factor.

This interaction is incorporated into the Hamiltonian in the form

$$-\beta_n \vec{H} \cdot \tilde{g}_n' \cdot \vec{I} \qquad (18)$$

where β_n is the nuclear magneton.

Referred to its principal axes this becomes

$$\beta_n (g_{nx}' H_x I_x + g_{ny}' H_y I_y + g_{nz}' H_z I_z) \qquad (19)$$

In the case of axial symmetry this becomes

$$\beta_n g'_{n_{\parallel}} H_z + \beta_n g'_{n_{\perp}} (H_x I_x + H_y I_y) \qquad (20)$$

At H = 3000 gauss the interaction energy is $\sim 10^{-4} cm^{-1}$ for $^{53}Cr^{3+}$.

III 5 The Zeeman Interaction

The interaction between the effective spin of the ion and the applied magnetic field is called the Zeeman effect. In the iron group elements the electrons have their spin and orbital magnetic moments, $\vec{\mu}_S$ and $\vec{\mu}_L$, coupled via the Russell-Sanders mechanism. In this case the total angular momentum is defined as the vector sum of the orbital and spin angular momenta. The magnetic moment of the coupled system is

$$\vec{\mu}_J = -g \frac{e}{2mc} \vec{P}_J \qquad (21)$$

where

$\vec{P}_J = \hbar\sqrt{J(J+1)}$

$\vec{J} = \vec{L} + \vec{S}$

m is the electron mass

e is the electronic charge

c is the velocity of light

g is the spectroscopic splitting factor

The interaction of the total magnetic moment $\vec{\mu}_J$ of the atom with the external magnetic field is

$$H_{Zeeman} = -\vec{\mu}_J \cdot \vec{H} \tag{22}$$

$$= g \frac{e}{2mc} \vec{P}_J \cdot \vec{H}$$

$$= g \frac{e\hbar}{2mc} \vec{J} \cdot \vec{H} \tag{23}$$

$\frac{e\hbar}{2mc} = \beta$ is the Bohr magneton so that we can write

$$H_{Zeeman} = g\beta\vec{J} \cdot \vec{H} \tag{24}$$

The g-value for a paramagnetic ion in a solid is in general a tensor quantity reflecting the symmetry of the crystalline electric field. Also, since the ground state of the ion is an orbital singlet we can write equation (24) as

$$\beta\vec{H} \cdot \tilde{g} \cdot \vec{S} \tag{25}$$

In the principal axes system we can write this as

$$\beta(g_x H_x S_x + g_y H_y S_y + g_z H_z S_z) \tag{26}$$

and for the case of axial symmetry we have

$$\beta g_{\parallel} H_z S_z + \beta g_{\perp} (H_x S_x + H_y S_y) \tag{27}$$

The magnitude of the Zeeman interaction for the case of S = 3/2 and H = 3000 gauss is of the order of 10^{-1} cm^{-1}.

III 6 The Complete Spin Hamiltonian

Grouping together the terms given in the above sections, we have the following spin Hamiltonian which describes the energy levels of the ground state orbital singlet of $^{53}Cr^{3+}$ in a crystalline electric field of axial symmetry plus an external magnetic field:

$$\begin{aligned}\mathcal{H} &= g_{\parallel}\,\beta\,S_z H_z + g_{\perp}\,\beta(H_x S_x + H_y S_y) \\ &+ D\left[S_z^2 - \tfrac{1}{3}S(S+1)\right] + AS_zI_z \\ &+ B(S_xI_x + S_yI_y) + Q'\left[I_z^2 - \tfrac{1}{3}I(I+1)\right] \\ &- g'_{n_{\parallel}}\,\beta_n H_z I_z - g'_{n_{\perp}}\,\beta_n(H_xI_x + H_yI_y) \qquad (28)\end{aligned}$$

All the terms in this expression are regarded as having the same principal axes.

In the application of this spin Hamiltonian to the problem at hand the matrix form is used. Since $S = 3/2$ and $I = 3/2$ for $^{53}Cr^{3+}$, and $(2S + 1)(2I + 1) = 16$, this means that we have a 16 x 16 matrix. The matrix elements are tabulated in table 8 in appendix 1. Their exact form and use in the calculations is discussed in the following chapter.

III 7 ESR Transitions and Linewidths

Transitions in which electrons move from one M_s level to another (following the selection rule $\Delta M_s = \pm 1$) are called electron

spin resonance transitions. This effect was discovered by Zaviosky in 1945[11]. The energy necessary for these transitions is obtained from the microwave field when the magnetic field has split the levels by an amount equal to (see figure 2) the frequency of the microwaves times h. The electron now gives up its extra energy, eventually to the crystal lattice or possibly first transferring some of the energy to another paramagnetic ion. These interactions can be thought of as relaxation effects which play a great part in determining the suitability of a crystal for study.

Van Vleck[12] is mainly responsible for the theory concerning the rate at which a spin exchanges a whole quantum of energy with the lattice, the spin-lattice relaxation time. The mechanism envisioned is one in which the thermal vibrations of the lattice give rise to fluctuations crystalline electric field. The spin-orbit coupling plays an essential role as the means by which the spin of the paramagnetic ion feels the effect of the thermal vibrations. The spin-lattice relaxation time τ is strongly temperature dependent, sometimes as T^{-5}, becoming larger as the temperature is reduced. The theory also shows that τ depends very markedly on the separation between the ground state and the first exited state. If the separation is large then τ is also. The practical consequences of this arise from the fact that the lifetime of the state is related to the width of the observed line. This can be seen from the uncertainty relation

$$\Delta E \cdot \Delta t \sim h/2\pi \qquad (29)$$

where

ΔE is the width of the energy level

and Δt is the lifetime of the state.

A second relaxation process is the spin-spin interaction. In this case the magnetic moment of each ion is regarded as precessing about the external magnetic field H, and can thus be resolved into a fixed component in the direction of H, and a rotating component perpendicular to H. These two components cause the neighbouring ions to behave as if they were in a slightly different external magnetic field. If the rotating part of the field has the same frequency as the other paramagnetic ions, there will be a couple acting on the steady component of the magnetic moment of the latter ion tending to change its direction. Thus two types of broadening are introduced: first, a broadening which is of the same type as that which arises from an inhomogeneous magnetic field; second, a resonance broadening caused by the tendency to reduce the lifetime of a given state.

These latter effects are not temperature dependent and can only be affected by changing the density of the paramagnetic centres.

III 8 ENDOR Transitions

The electron nuclear double resonance (ENDOR) technique was invented by Feher in 1956[13,14]. To observe ENDOR the magnetic field is adjusted to the centre of an electron spin resonance line and enough power is applied to nearly equalize the population of the upper level

which, at thermal equilibrium, is less densely populated than the lower level according to the relation

$$\frac{N_L}{N_U} = \exp \frac{\Delta E}{kT} \sim 1 + \frac{\Delta E}{kT} \qquad (30)$$

where

N_L is the number of spins in the lower level and

N_U is the number of spins in the upper level

For our experimental conditions of liquid helium temperature and $\Delta E \sim 9.4$ GHz there are roughly 100 times more electrons in the lower state. The degree of saturation depends on the balance between the energy density in the cavity and the rate at which the electrons return to the ground state through relaxation processes. After the desired level of saturation is achieved a radio frequency field, approximately equal in energy to the splitting between the nuclear levels is slowly frequency swept through the range of the transitions. Now, electrons will move to the higher (or lower) nuclear levels via $\Delta M_I = \pm 1$ transitions and desaturate the upper ESR state thus causing ESR transitions ($\Delta M_s = \pm 1$) to reoccur, removing energy from the microwave field. This is shown in figure 3. Thus the nuclear transition is detected via the electron spin resonance, and the frequency where this occurs is recorded. The ENDOR phenomenon causes an increase in the resolution of the nuclear levels to be measured by an amount equal to the ratio of the electronic to the nuclear magneton, which in practice is a factor of about 10^3.

In making calculations from ESR transitions measurements must

be made of the positions of successive lines and the parameters are deduced from the differences in these positions. The accuracy of these measurements is limited by linewidth. The ENDOR technique overcomes this difficulty by the direct measurement of the nuclear levels. ENDOR measurements may be made even if the hyperfine structure is totally unresolved for the ESR spectrum. The resulting increase in accuracy is of the order of 10^3.

There are several sources of broadening for the double resonance lines: 1) Stray fields exist as for ESR but they have a much less significant effect. This is because the 10 gauss (approx.) stray field is perturbing a 1/2 million gauss field produced by the electron instead of a 3000 gauss external field at the electron. 2) Other effects, including the spin-lattice interactions do not significantly affect the ENDOR linewidths.

Using ENDOR, we can accurately calculate the hyperfine interaction parameters A, B, Q' and g_n', previously discussed.

CHAPTER IV

EQUIPMENT

IV 1 Introduction

In the course of this work two X-band microwave spectrometers were used. One spectrometer was of commercial design and the other was constructed in this laboratory by Danilov and Manoogian[15,16]. Modifications made by this author to the latter spectrometer involved the rearrangement of the microwave circuit, which resulted in the removal of 40% (12 feet) of its original length. Also, the placing of aluminum foil gaskets between the flanges of the individual components allowed better electrical contacts to be made. The net effect of these changes was to increase significantly the stability of the spectrometer. Both spectrometers had the capacity to operate in the range of room to liquid helium temperature. They are described in the following two sections.

IV 2 X-Band Superheterodyne Spectrometer used in ENDOR studies

This spectrometer, shown schematically in figure 4 was constructed using commercially available electronic components and a combination of commercial and "home-made" microwave components. The

Figure 4: A schematic diagram of the superheterodyne spectrometer

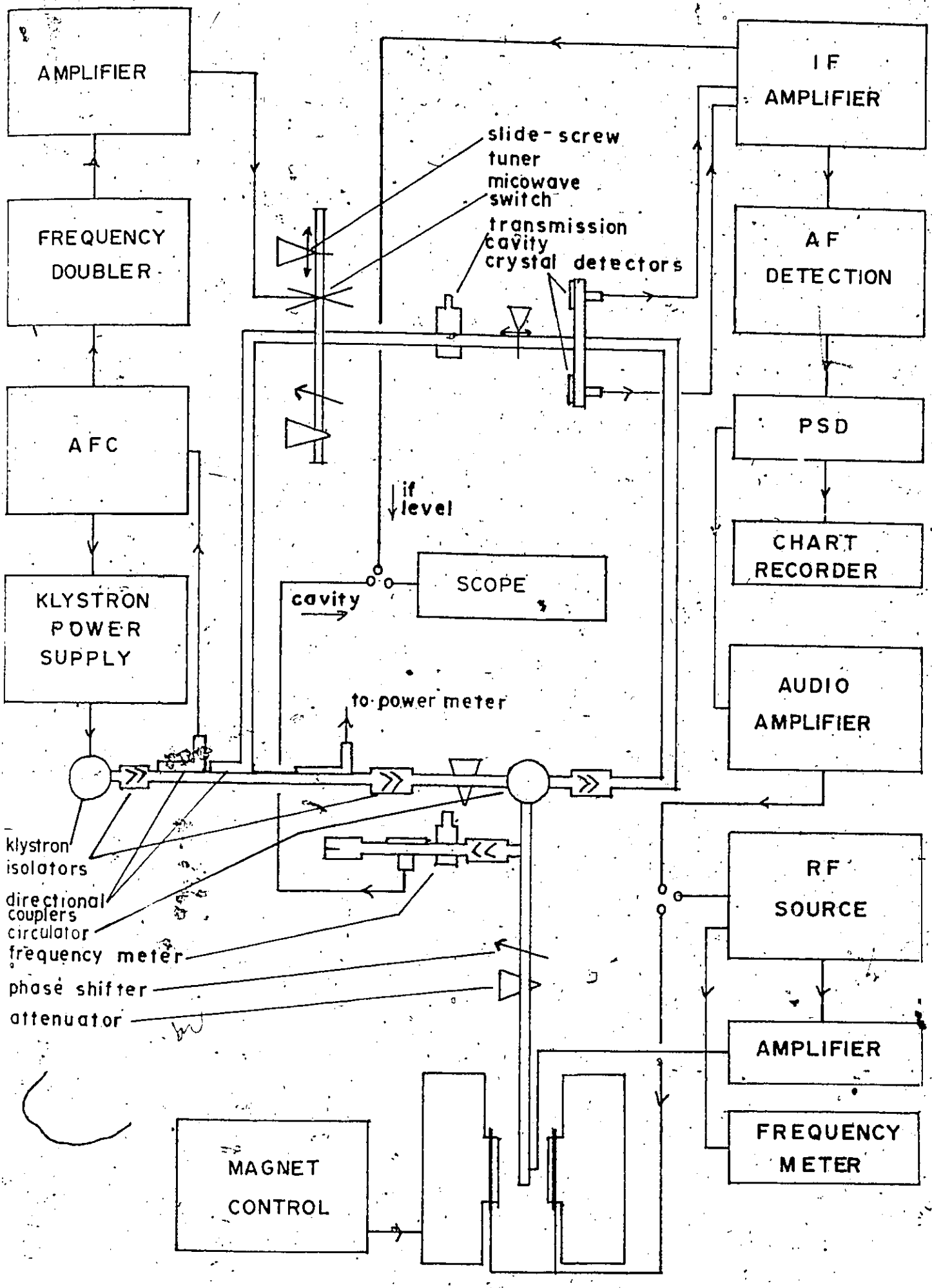
AMPLIFIER
FREQUENCY DOUBLER
AFC
KLYSTRON POWER SUPPLY
IF AMPLIFIER
AF DETECTION
PSD
CHART RECORDER
AUDIO AMPLIFIER
RF SOURCE
AMPLIFIER
FREQUENCY METER
MAGNET CONTROL
slide-screw tuner
micowave switch
transmission cavity
crystal detectors
if level
SCOPE
cavity
to power meter
klystron isolators
directional couplers
circulator
frequency meter
phase shifter
attenuator

source of microwave power in this spectrometer is a low noise Varian X-band reflex klystron capable of producing about 350 mW of power in a narrow range of frequencies centred at about 9.3 GHz. The method of operation is as follows: the klystron is tuned to the resonant frequency of the sample cavity and then stabilized with reference to a high harmonic of a temperature controlled crystal oscillator. The frequency stabilized microwave power is fed into two parts of the microwave circuit. In one part power is fed by a 10 db coupler to a magic-T, one arm of which contains a microwave switch. This microwave switch is activated by a 30 MHz signal derived from an auxilliary output of the frequency stabilizer. Consequently, side bands are produced at 30 MHz above and below the carrier frequency. One of these side-bands is selected by the careful tuning of a transmission cavity in another arm of the magic-T. Thus microwave power, 30 MHz away from the carrier is fed into the H-arm of a second magic-T which contains two balanced crystals and is in effect a frequency mixer. The carrier, at the centre frequency, is reflected from the sample cavity and is received in the E-arm of this magic-T. The two signals are then mixed and the intermediate frequency (I.F.) is detected. In the detection of paramagnetic absorption, the microwave bridge, consisting of a precision attenuator and a precision phase shifter, is close to balance so that off the resonance point only a small constant microwave level

is present in the E-arm of the mixer. When energy absorption occurs the reflection coefficient changes, further unbalancing the microwave bridge. This in turn produces a higher microwave level in the E-arm and thereby a proportionally larger I.F. signal is produced.

The magnetic field is modulated at a frequency of 200 Hz and an amplitude of $\sim$ 5 gauss by employing Helmholtz coils mounted on the magnet pole faces. The 200 Hz is derived from an output of the phase sensitive detector (PSD) and is amplified before being applied to the coils. As the external magnetic field is swept slowly through the resonance point of an ESR line the effect of this 200 Hz signal is to amplitude modulate the reflected power from the cavity. This is shown in figure 5. The I.F. is consequently amplitude modulated at this same frequency. After I.F. amplification, a crystal detector picks up the 200 Hz signal riding on the I.F. level. This signal, slowly varying in both magnitude and phase at the rate of the field sweep, is then fed into the PSD. The output of the PSD is fed into a strip-chart recorder. The output of the PSD gives the derivative of the absorption or dispersion, depending on the type of imbalance at the microwave bridge. The PSD could be adjusted for sensitivity, time constant and Q-factor to give the optimum signal-to-noise ratio.

The ENDOR detection system is slightly different. The magnetic field is centred on an ESR absorption line which is then partially saturated by increasing the amount of microwave power in

Figure 5: The effect of modulation. The diagram is drawn for ESR; for ENDOR the x-axis becomes frequency.

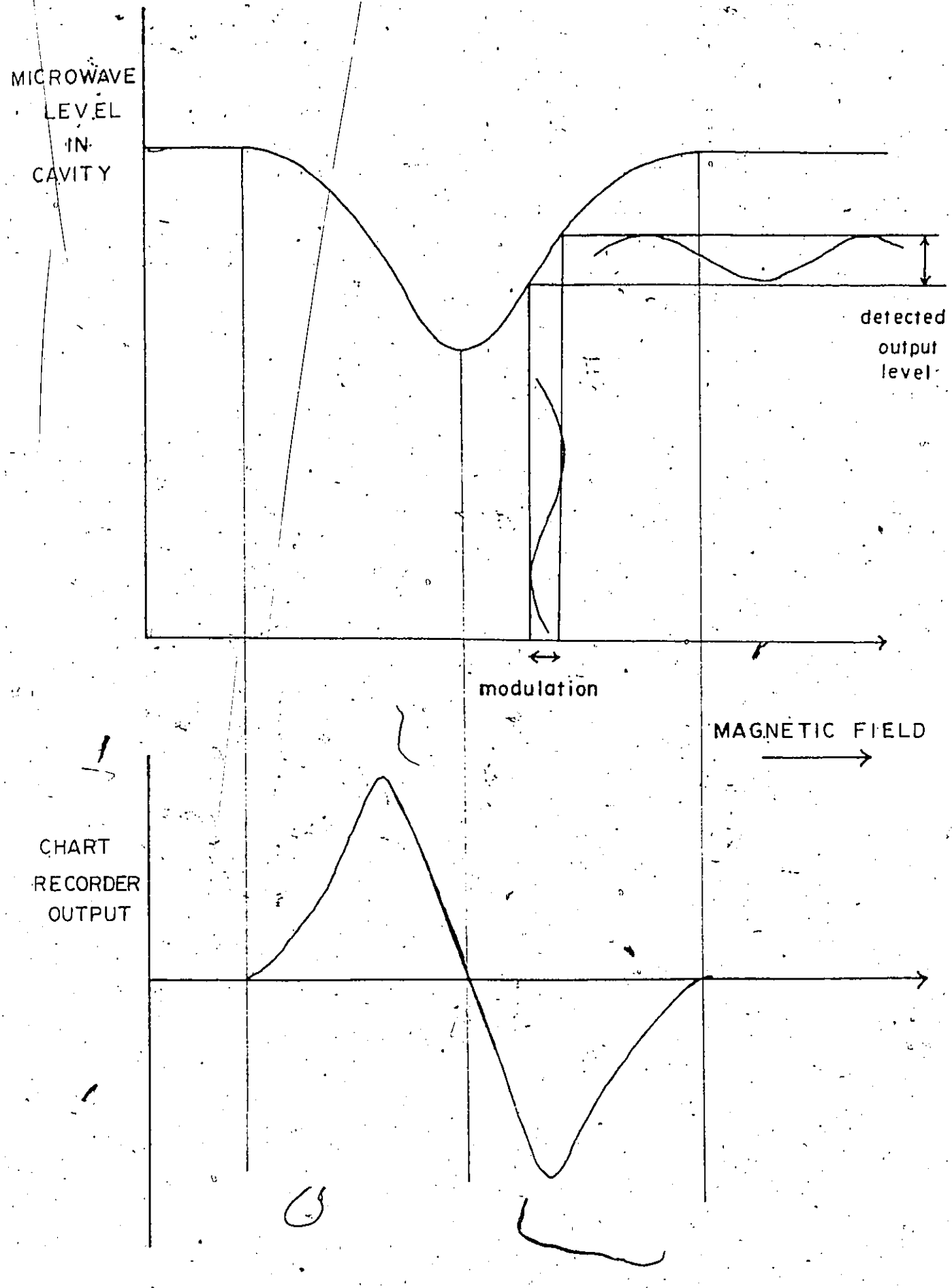
MICROWAVE LEVEL IN CAVITY
detected output level
modulation
MAGNETIC FIELD
CHART RECORDER OUTPUT

the sample cavity. With the magnetic field held constant and no field modulation employed, radio frequency energy in the 75 MHz range is fed through a small coil surrounding the sample and is slowly frequency swept. The 200 Hz signal from the PSD is used to frequency modulate this radio frequency, normally with an amplitude of modulation of 75 kHz. When absorption occurs, the microwave bridge is unbalanced and the microwave power reflected from the cavity is again amplitude modulated at 200 Hz and detected as in the case of ESR. Due to the reduction in the microwave circuit length etc., previously described, a given level of stability for the spectrometer increased from minutes to hours, increasing the accuracy of the measurements.

IV 3 The Commercial X-Band Spectrometer

This spectrometer, used for ESR measurements at room temperature, was manufactured by Hilger and Watts Co. Ltd., of England. The microwave source in this equipment was a reflex klystron capable of supplying 35 mW of power at a frequency of approximately 9.5 GHz. This spectrometer did not operate on the superheterodyne principle. The method of operation was similar to the previously described case except that the field modulation was accomplished by means by a small coil of wire in the microwave cavity which was attached to an oscillator producing a 100 kHz, 1 gauss modulation.

IV 4 The Microwave Cavities

A cylindrical cavity which operated in the TE_{011} mode was used with the commercial Hilger and Watts spectrometer for the room temperature measurements.

The ENDOR cavity used with the superheterodyne spectrometer was rectangular and operated in the TE_{014} mode. This cavity was designed to resonate at liquid helium temperature at the highest klystron power mode. An adjustable matching screw was also inserted just above the iris to fine tune the cavity Q for different crystals. The Q of the cavity at liquid helium temperature was about 6000 unloaded and 4500 loaded (with a crystal). The resonant frequency was near 9.4 GHz.

To maintain this high Q the ENDOR coil had to be positioned precisely in the $\lambda/2$ plane. (see figure 6). The crystal support had accurately machined surfaces to hold the crystal in either the [111] direction or in the [111] plane relative to the externally applied magnetic field.

IV 5 The Magnet and Magnetic Field Measurement

The magnetic field was produced by an 8 inch Newport magnet which is current regulated for stability. The field was observed to be very homogeneous between the pole faces and the field vs current behaviour was nearly linear in the experimental range.

The magnetic field was measured by proton nuclear magnetic

Figure 6: The ENDOR x-band cavity; showing sample holder, ENDOR coil support and magnetic fields at sample.

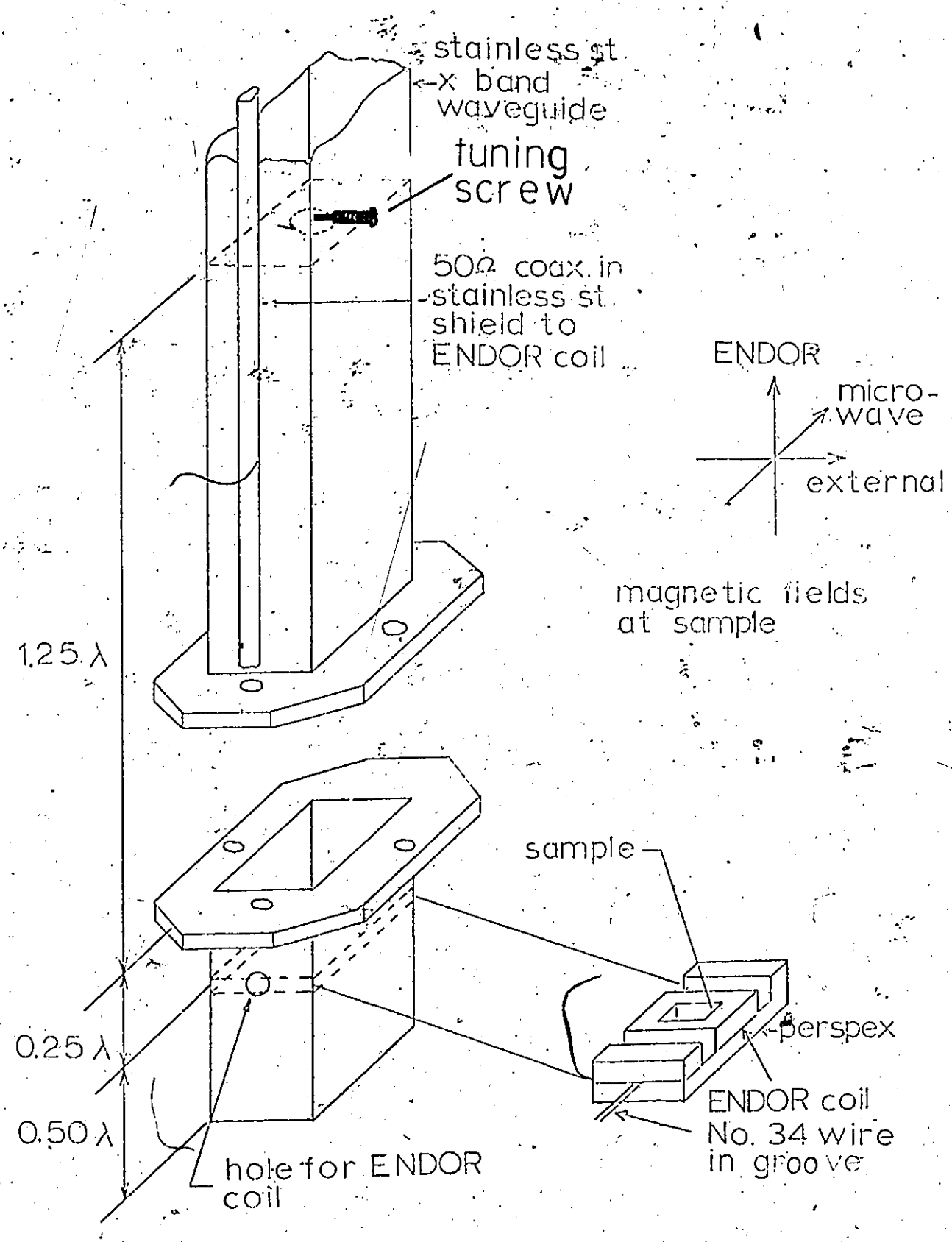
stainless st.
x band
waveguide
tuning
screw
50Ω coax. in
stainless st.
shield to
ENDOR coil
ENDOR
micro-
wave
external
magnetic fields
at sample
1.25 λ
sample
perspex
0.25 λ
0.50 λ
ENDOR coil
No. 34 wire
in groove
hole for ENDOR
coil

resonance (NMR). The proton source was a vial of water which was doped with copper sulfate. The magnetic field was modulated at 60 Hz for observation of the proton resonance, and the signal was monitored on an oscilloscope, the horizontal input of which was connected to a 60 Hz source and a phase shifter. The frequency at which proton resonance occurred was measured by a frequency counter. The strength of the magnetic field is obtained from the expression

$$H(\text{k gauss}) = \frac{\nu(\text{MHz})}{4.25759} \qquad (31)$$

where ν is the proton resonance frequency and 4.25759 is the frequency for proton resonance in a 1 kgauss magnetic field.

IV 6 Dewar System

A standard double dewar system was employed, the outer dewar holding liquid nitrogen, the inner, liquid helium. The stainless steel waveguide and brass cavity were immersed in the liquid. Small holes drilled in the waveguide allowed helium to directly immerse the sample. Two litres of helium was enough for approximately six hours of continous operation.

CHAPTER V

EXPERIMENTAL RESULTS AND CALCULATIONS

V 1 Introduction

This chapter deals with the ESR and ENDOR measurements and the calculations made using the data to find the various parameters of the spin Hamiltonian.

V 2 ESR Results

The ESR of both the rubidium and caesium aluminum alums was studied to determine the values of g and D of the chromium magnetic complexes in the crystals. This was done at room, liquid nitrogen and liquid helium temperatures. Angular variation studies showed that the chromium spectral lines in the Rb and Cs aluminum alums consisted of four differently oriented but otherwise equivalent magnetic complexes. A typical complex consists of three fine structure lines, each split into four hyperfine lines. The $^{53}Cr^{3+}$ hyperfine lines in RbAℓ alum were unresolved at room temperature but were resolved at 4.2°K. The room temperature ESR spectrum of the Rb Aℓ alum is shown in figure 7. The hyperfine lines in the CsAℓ alum were resolved at both temperatures An example of one of these resolved groups of hyperfine lines is shown in figure 8.

figure 7: The room temperature, z-axis, ESR spectrum of $^{53}Cr^{3+}$ in RbAl alum


1978.47
3429.59
4932.87
H (gauss)

Figure 8: The helium temperature ESR spectrum of the low field group of hyperfine lines of $^{53}Cr^{3+}$ in CsAℓ alum in the z-axis orientation, indicating the centres of the hyperfine lines

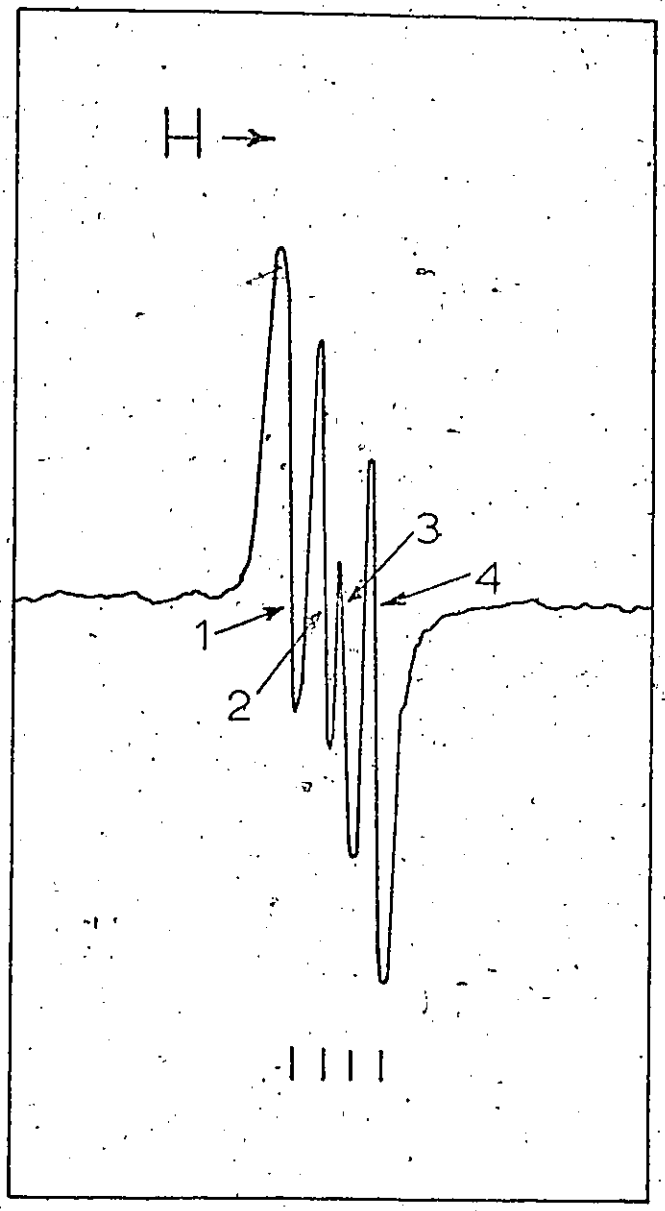
H
1
2
3
4

In general, the magnetic axes of a given complex are obtained when the fine structure lines show extrema in their separation with respect to the external magnetic field direction. This occurs when the external magnetic field points along one of the three mutually perpendicular axes of the crystal field tensor for one of the complexes. One such extremum is found when the external magnetic field points along the crystal [111] direction. This direction is termed the z-axis. Also, when the external magnetic field was anywhere on the cone defined by the [111] direction, the ESR spectrum for the complex in question was identical, indicating axial symmetry.

Measurements were made as follows: with the crystal and magnet properly oriented and the spectrometer properly tuned, the magnetic field was swept from 0 to about 6 kilogauss, to get an idea of the pattern of the spectrum. The field was then lowered to a value just under the first group to be measured and allowed to increase slowly to the centre point of a fine structure group, or if resolved, to the centre of each hyperfine line. The sweep was then stopped, the field modulation turned off and the field position(s) of the line(s) was(were) measured. After all the field positions were measured the frequency of the microwave field was read from a calibrated wavemeter.

The g-factor was determined from the relation

$$h\nu = g\beta H_0 \qquad (32)$$

where

$$H_o = \tfrac{1}{2}(H_1 + H_3) \tag{33}$$

H_1 and H_3 are the field values of the centres of the extrema of the z-axis spectrum.

The D parameter was determined from the relation.

$$D = \tfrac{1}{4}(H_3 - H_1) \tag{34}$$

The sign of the D parameter is then dependent upon the ordering of H_1 and H_3. Theory tells us that when the magnetic field is directed along the z-axis

$$\left.\begin{aligned} H_1 \quad & = \quad H_o - 2D \\ & M_s(+1/2 \rightarrow 3/2) \\ H_2 \quad & = \quad H_o \\ & M_s(-1/2 \rightarrow +1/2) \\ H_3 \quad & = \quad H_o + 2D \\ & M_s(-3/2 \rightarrow -1/2) \end{aligned}\right\} \tag{35}$$

for the case of axial symmetry. The identification of H_1 and H_3 were accomplished by comparing the relative intensities of the low and high

field groups of lines at 4.2°K with reference to their relative intensities at room temperature. The thermal distribution of electrons in the various levels at 4.2°K causes the lowest lying transition to occur more intensely than the highest lying transition, for the same unsaturated input power and tuning conditions. For example, if the low field line is larger, a $-\frac{3}{2} \rightarrow -\frac{1}{2}$ transition is indicated identifying H_3 as the low field line. Since $H_3 = H_o + 2D$, D in this case is negative as for the caesium alum. Figure 9 illustrates this. The values found for the g-factor and the D parameter are listed in Table 1.

Table 1

Parameters for $^{53}Cr^{3+}$ in RbAℓ alum			Parameters for $^{53}Cr^{3+}$ in CsAℓ alum		
Temp.	D ($\times 10^{-4}$ cm^{-1})	g	Temp.	D ($\times 10^{-4}$ cm^{-1})	g
Room	680.80	1.9742	Room	-771.75	1.9763
Nitrogen	352.48	1.9775	Nitrogen	-732.51	1.9782
Helium	351.29	1.9759	Helium	-725.67	1.9788

Figure 9: Energy vs Magnetic Field plots showing the splitting of a $^4S_{3/2}$ state for D positive, D negative and D = 0.

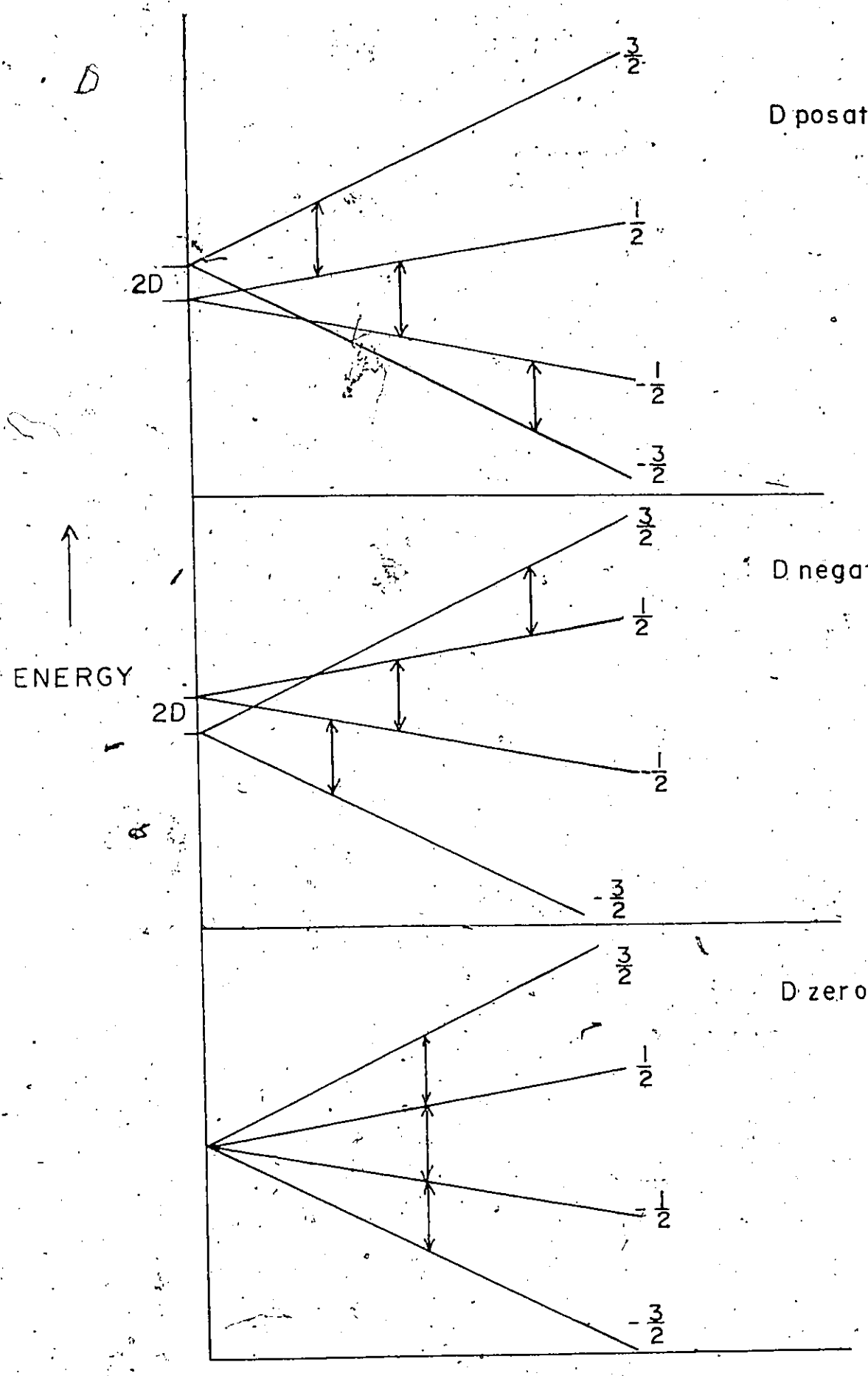
D positive
3/2
1/2
2D
-1/2
-3/2
D negative
3/2
1/2
ENERGY
2D
-1/2
-3/2
D zero
3/2
1/2
-1/2
-3/2
MAGNETIC FIELD

Figure 10 shows a plot of D vs T for both alums. It was postulated by McGarvey[17] that the D parameter is related to the extension or compression of the octahedron of waters surrounding the paramagnetic ion. The temperature dependancy was studied to learn more about the D parameter. D vs T was nearly linear for the case of the CsAℓ alum but for the RbAℓ alum it was markedly non-linear.

V 3 ENDOR Results

ENDOR measurements were made at 4.2°K in the 25 and 75 MHz frequency ranges along the z and a perpendicular direction of a typical magnetic complex in both the RbAℓ and CsAℓ alums. All ENDOR transitions in the $M_S(\pm\frac{1}{2} \rightarrow \pm 3/2)$ groups were measured along the z and perpendicular directions while those of the $M_S(-\frac{1}{2} \rightarrow \frac{1}{2})$ groups were measured for the z direction only. The measurements were made by setting the magnetic field to the centre of each of the four hyperfine lines of a group. Tables 2 and 3 give the 75 MHz readings along with the corresponding calculated values and their respective differences. The 25MHz readings are listed in Tables 9 and 10 in Appendix 3. Figures 11 and 12 show tracings of the chart recordings of the 75 MHz transitions for $^{53}Cr^{3+}$ in the CsAℓ and RbAℓ alums, respectively.

Figure 10: D vs T for $^{53}Cr^{3+}$ in RbAℓ alum and CsAℓ alum. The coordinates are listed in Table 1, page 40.

Note: for a further clarification of RbAℓ alum curve see post oral Discussion.

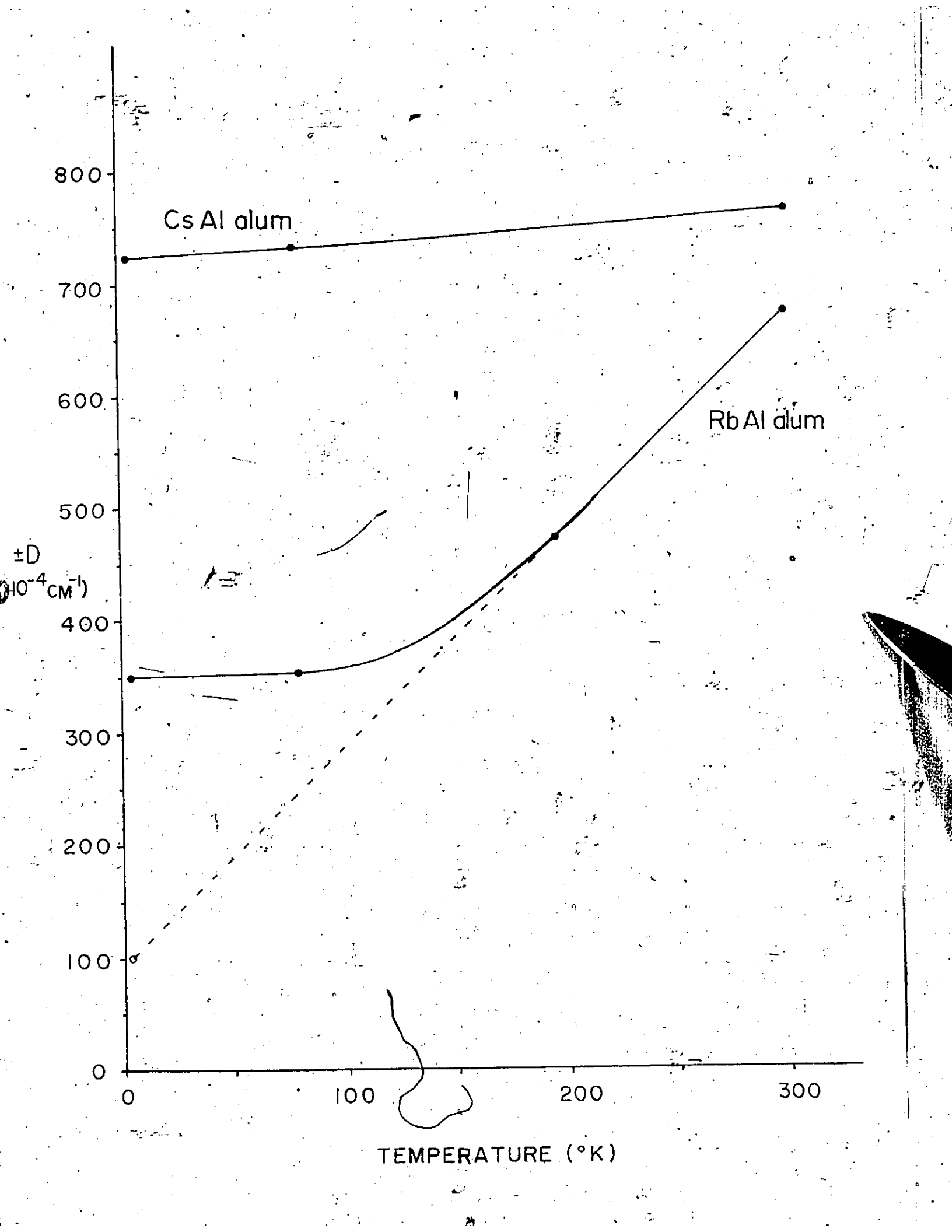
800
700
600
500
400
300
200
100
0
Cs Al alum
Rb Al alum
±D
(10⁻⁴cm⁻¹)
0
100
200
300
TEMPERATURE (°K)

Figure 11 : The 75 MHz ENDOR chart recordings for $^{53}Cr^{3+}$ in CsAℓ alum at 4.2°K (a) are from the low field group, $M_s(-3/2 \rightarrow -1/2)$ (b) are from the high field group, $M_s(1/2 \rightarrow 3/2)$; H along the z direction.

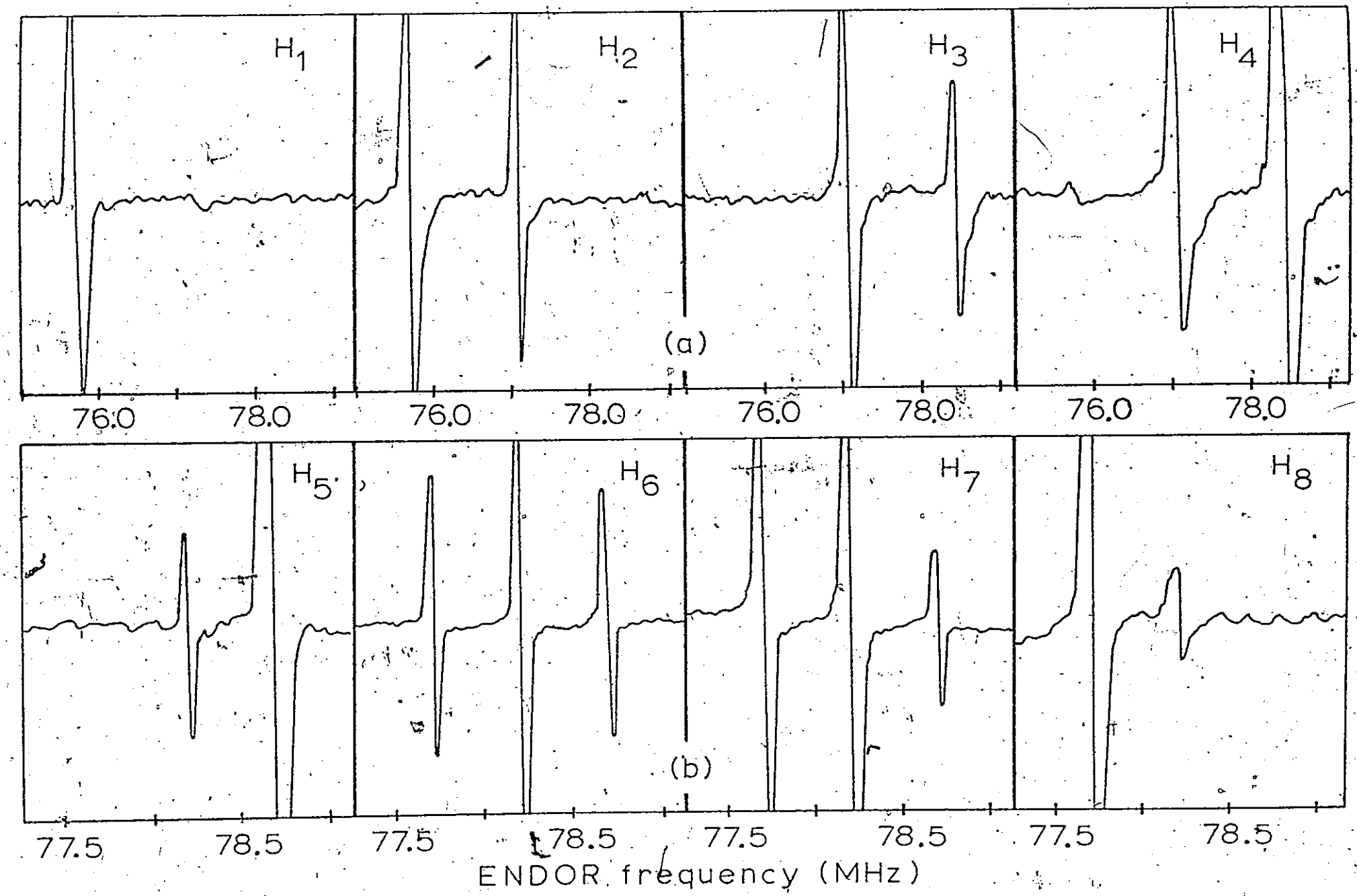
H1
H2
H3
H4
(a)
76.0
78.0
76.0
78.0
76.0
78.0
76.0
78.0
H5
H6
H7
H8
(b)
77.5
78.5
77.5
78.5
77.5
78.5
77.5
78.5
ENDOR frequency (MHz)

Figure 12: The 75MHz ENDOR chart recordings for $^{53}Cr^{3+}$ in RbAℓ alum at $4.2^{o}K$. (a) are from the low field group, $M_s(1/2 \rightarrow 3/2)$. (b) are from the high field group, $M_s(+3/2 \rightarrow -1/2)$; H along the z direction.

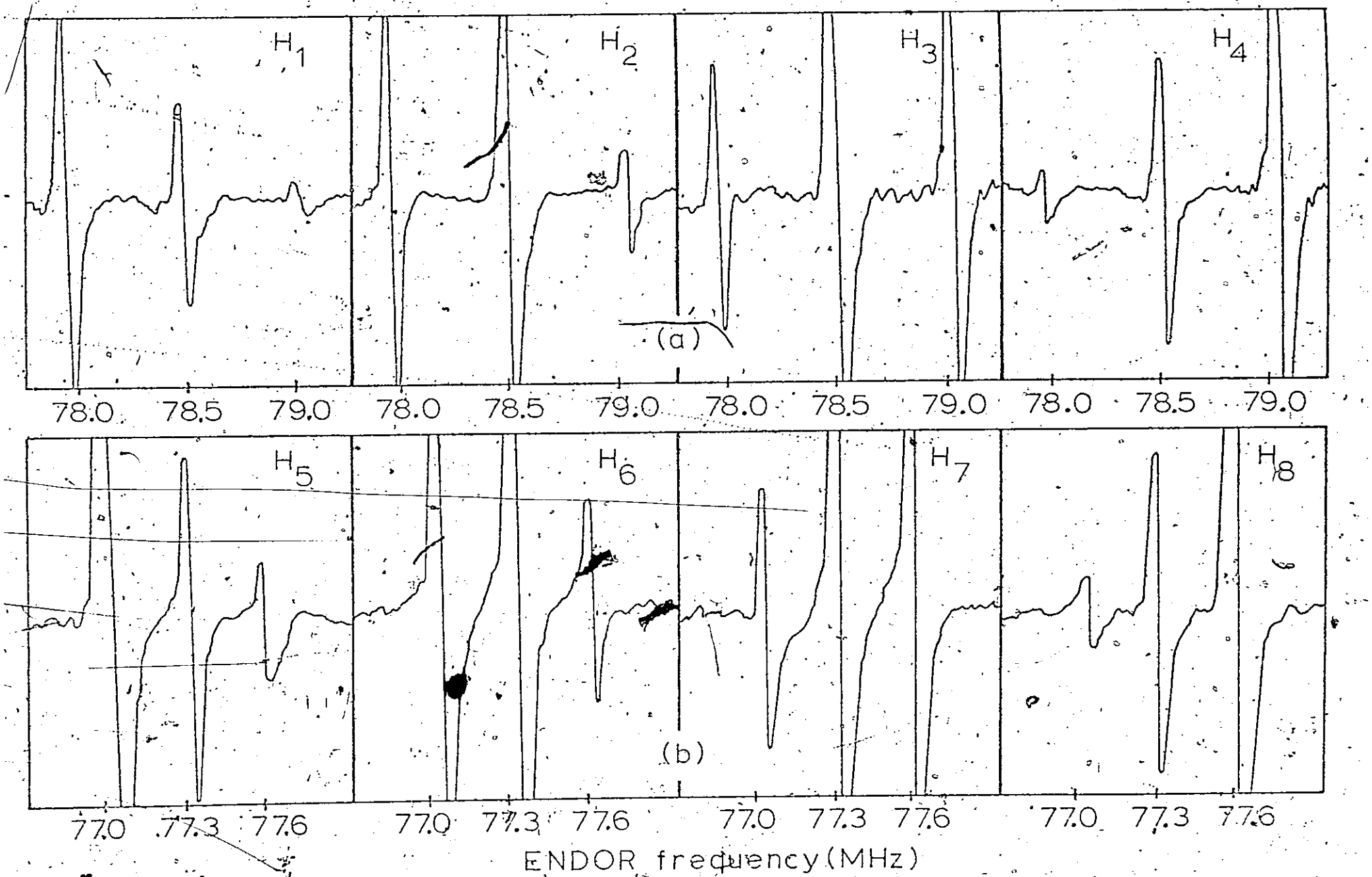
H1
H2
H3
H4
(a)
78.0
78.5
79.0
H5
H6
H7
H8
(b)
77.0
77.3
77.6
ENDOR frequency (MHz)

Table 3

RUBIDIUM ALUM

Z-DIRECTION--- ENDOR FREQUENCIES (MHz)

FIELD (kg)	CALCULATED	MEASURED	DIFFERENCE
2.58113	77.963	77.960	.003
	78.515	78.517	.002
2.60403	77.971	77.969	.002
	78.525	78.522	.003
	79.087	79.084	.003
2.62258	77.979	77.973	.006
	78.531	78.532	.001
	79.092	79.092	.000
2.64131	77.990	77.995	.005
	78.536	78.542	.006
	79.092	79.093	.001
4.09246	77.341	77.328	(.013)
	77.035	77.036	.001
4.11228	77.642	77.640	.002
	77.336	77.338	.002
	77.030	77.033	.003
4.13443	77.634	77.643	.009
	77.328	77.333	.005
	77.027	77.024	.003
4.15775	77.626	77.635	.009
	77.320	77.324	.004
	77.019	77.022	.003

Average Diff. = .003 MHz
(excluding(0.013))

⊥-DIRECTION--- ENDOR FREQUENCIES (MHz)

FIELD (kg)	CALCULATED	MEASURED	DIFFERENCE
2.96400	77.564	77.556	.008
	77.063	77.052	.011
	76.566	76.547	.019
2.98277	77.564	77.562	.002
	77.060	77.058	.002
	76.566	77.546	.020
3.00048	77.559	77.572	.013
	77.060	77.058	.002
	76.563	76.543	.020
3.02213	77.556	77.572	.016
	77.052	77.053	.001
3.71304	77.924	77.939	.015
	78.288	78.291	.003
	78.668	78.650	.018
3.73190	77.939	77.944	.005
	78.299	78.299	.000
	78.668	78.654	.014
3.75022	77.942	77.941	.001
	78.309	78.305	.004
	78.681	78.663	.018
3.76974	77.958	77.932	.026
	78.309	78.300	.009
	78.687	78.666	.021

Average Diff. = .009 MHz

Table 3.

CAESIUM ALUM

Z-DIRECTION--- ENDOR FREQUENCIES (MHz)				⊥-DIRECTION--- ENDOR FREQUENCIES (MHz)			
FIELD (kg)	CALCULATED	MEASURED	DIFFERENCE	FIELD (kg)	CALCULATED	MEASURED	DIFFERENCE
1.79346	77.203	77.201	.002	2.59024	76.868	76.890	.022
	75.847	75.839	.008		77.755	77.760	.005
1.81171	77.200	77.193	.007	2.60946	76.897	76.914	.017
	75.837	75.836	.001		77.773	77.773	.000
1.82998	78.548	78.547	.001		78.634	78.649	.015
	77.190	77.189	.001	2.62826	77.792	77.797	.005
	75.839	75.679	(.160)		78.660	78.665	.005
1.84759	78.537	78.540	.003	2.64770	77.813	77.806	.007
4.89620	78.835	78.836	.001		78.679	78.683	.004
	78.360	78.363	.003	4.10948	77.024	77.022	.002
4.91499	78.840	78.848	.008	4.12792	77.026	77.024	.002
	78.368	78.371	.003	4.14577	77.024	77.022	.002
	77.894	77.902	.008	4.16468	77.024	77.018	.006
4.93401	78.854	78.853	.001				
	78.368	78.375	.007				
	77.899	77.905	.006				
4.95304	78.374	78.374	.000				
	77.904	77.907	.003				

Average Diff. = .004 MHz
(excluding (0.160))

Average Diff. = 0.007 MHz

V 4. Finding the Spin Hamiltonian Parameters

Using equation (28) all the elements of the spin Hamiltonian matrix were calculated. These are listed in Table 8, Appendix 1. The matrix was then diagonalized to second order using perturbation theory. The second order equations have the general form

$$E = E_{\text{diagonal}} + E_{\text{first order}} \quad E_{\text{second order}} \tag{36}$$

where E_{diagonal} is a diagonal matrix element, $E_{\text{first order}}$ is the expectation value of the perturbation in the uperturbed basis and $E_{\text{second order}}$ is a term related to the off-diagonal elements. These can be written as

$$E = E_{\text{diagonal}} + \langle m|\mathcal{H}|m\rangle + \sum_n \frac{|\langle m|\mathcal{H}|n\rangle|^2}{E_m^o - E_n^o} \tag{37}$$

Thus 16 analytical expressions for the hyperfine energy levels correct to second order are produced. Expressions for adjacent hyperfine levels can now be subtracted to give the ENDOR transition frequencies. Twelve such expressions can be obtained but only those of the 75 MHz range were used because these transitions were more accurately measured. These six expressions are listed in Table 4, for H along the z direction.

Table 4

Analytical expressions for the 75 MHz transitions

For the M_s = +3/2 multiplet:

$$M_I(\tfrac{1}{2} \rightarrow 3/2) \quad h\nu = 3/2A + 2Q' - g_n'\beta_n H_z - 9/4B^2 \cdot \frac{1}{g_{\parallel}\beta H_z + 2D}$$

$$M_I(-\tfrac{1}{2} \rightarrow \tfrac{1}{2}) \quad h\nu = 3/2A - g_n'\beta_n H_z - 3/4B^2 \cdot \frac{1}{g_{\parallel}\beta H_z + 2D}$$

$$M_I(-3/2 \rightarrow -\tfrac{1}{2}) \quad h\nu = 3/2A - 2Q' - g_n'\beta_n H_z + 3/4B^2 \cdot \frac{1}{g_{\parallel}\beta H_z + 2D}$$

For the M_s = -3/2 multiplet

$$M_I(-\tfrac{1}{2} \rightarrow -3/2) \quad h\nu = 3/2A + 2Q' + g_n'\beta_n H_z - 9/4B^2 \cdot \frac{1}{-g_{\parallel}\beta H_z + 2D}$$

$$M_I(\tfrac{1}{2} \rightarrow -\tfrac{1}{2}) \quad h\nu = 3/2A + g_n'\beta_n H_z - 3/4B^2 \cdot \frac{1}{-g_{\parallel}\beta H_z + 2D}$$

$$M_I(3/2 \rightarrow \tfrac{1}{2}) \quad h\nu = 3/2A - 2Q' + g_n'\beta_n H_z + 3/4B^2 \cdot \frac{1}{-g_{\parallel}\beta H_z + 2D}$$

(H along the z direction).

In fact, only four equations are needed because only four parameters, A, B, Q' and g_n' are left to be evaluated. The analytical expressions were identified with the corresponding observed ENDOR frequencies by a study of the ordering and relative intensities of the

lines and the equations were solved. The approximate values calculated for Rb alum are given in Table 5. below.

Table 5

The Spin Hamiltonian Parameters for $^{53}Cr^{3+}$ in RbAℓ alum, correct to second order

A	=	52.0760	MHz
B	=	51.7341	MHz
Q'	=	-0.0207	x 10^{-4} cm^{-1}
g_n'	=	-0.3178	

Comparison of these values with the computer diagonalized final values shows the accuracy of this second order calculation. The values were similarly found for the CsAℓ alum.

Two computer programs were used for the exact fit of equation (28) to the ENDOR measurements. One program was used to fit the z axis measurements and the other for the perpendicular direction measurements. The method of fitting involved varying each starting parameter separately using the z-axis program until the values calculated by the computer using equation (28), diagonalized using the approximate

parameters, gave the best fit with the ENDOR frequencies obtained experimentally. In this process the A term was fitted first, followed by the Q' and the g_n' terms. The B term was then fitted along the perpendicular direction since it appears on the diagonal of the perpendicular matrix. The final step was to alternate back and forth between the z and perpendicular direction programs, varying individually all of the parameters until the best fit was obtained. The final values of the spin Hamiltonian parameters are listed in Table 6 below.

Table 6

The Exact Spin Hamiltonian Parameters

	$^{53}Cr^{3+}$ in RbAl alum	$^{53}Cr^{3+}$ in CsAl alum	Units
A	52.0720	51.6115	MHz
B	51.8215	52.3760	MHz
Q'	-0.0215	0.1545	$\times 10^{-4} cm^{-1}$
g_n'	-0.3170	-0.3140	
g_l	1.9759	1.9788	
D	351.29	-725.07	$\times 10^{-4} cm^{-1}$
			all at $4.2^{o}K$

The computer program listing for the z direction, and an example of the output is given in Appendix 2.

The measurements obtained at 25 MHz were not used in the fitting process because these lines had relatively low intensities, and were consequently measured with less accuracy than were the 75 MHz lines. The significant thing about them is simply that they were observed. In the ENDOR work on the corresponding gallium alums by Danilov and Manoogian[16], these lines were not observed. These lines could be useful if more than six parameters existed in the spin Hamiltonian, thus requiring more than six equations to obtain the approximate starting values.

V 5 Error Estimate

Errors in the readings were produced by misalignment of the magnet with the crystal magnetic axes, by the difficulty in measuring the exact centre of the ESR and ENDOR lines, and also because the NMR proton probe was not at the same point in the field as was the crystal. The error in measurement of the field position is estimated to be ±1 gauss and that of the ENDOR frequency, ±5 kHz. The error in magnetic field alignment is about ±0.5°. These errors combine in the computer fitting process, resulting in an average difference between the measured and theoretical values of 3.5 kHz for the z direction and 8 kHz for the perpendicular direction. Since most of the parameters were fitted using the z direction measurements, the accumulated error is closer to 3.5 kHz. This produes uncertainties of $\pm 0.001 \times 10^{-4}$ cm^{-1} in the A, B, Q' and V_{zz}'s, of $\pm 0.001 \times 10^{-4}$ barns for the Q's, of $\pm 0.05 \times 10^{-4}$ cm^{-1} for the D's and of ±0.001 in the g-values.

CHAPTER VI

DISCUSSION AND CONCLUSIONS

VI 1 Introduction

In this chapter the experimental results are discussed and put into a meaningful context. Possible relationships between the behavior of the crystals studied and the various spin Hamiltonian parameters found are presented. Comparisons are made between the findings of the present study and the other available data for the chromium ion in octahedrally coordinated sites.

VI 2 The D parameter and the Trigonal Distortion.

In both crystals studied, the chromium ion was found to exist in four equivalent, but differently oriented, magnetic complexes. In each complex the chromium ion is surrounded by an octahedron of water molecules which has a small trigonal distortion. McGarvey[17] has shown that a negative D value can be produced by a compression of the coordinated octahedron of waters along the trigonal axis, while a positive D would correspond to an extension of the octahedron. The above explanation is supported by an interpretation of the values of the D parameter measured by Manoogian and Leclerc[18] for the crystal guanidinium aluminum sulfate hexahydrate (GA&SH). In this crystal, two

inequivalent magnetic complexes exhibiting axial symmetry about the c axis of the crystal were found. In both complexes the $^{53}Cr^{3+}$ ion is surrounded by six waters as in the alums. The D parameters at room temperature were found to be negative and to increase in magnitude at low temperature. In the framework by McGarvey's study, we would interpret this to mean that the octahedron of waters around the chromium ion is trigonally compressed at room temperature and becomes even more compressed at low temperature. In GA&SH, which is a hexagonal crystal belonging to the space group P31m, the [111] direction of the octahedron points along the c axis of the crystal. Haussuhl and Trost[19] have found that the ratio of the thermal expansivity (at room temperature) along the c axis of the crystal to that along the a and b axes is about 9 to 1. Consequently, as the crystal is cooled, there is a net contraction along the [111] direction of the octahedron. It is the opinion of this author that regardless of whether the mechanism responsible for ths distortion is; (i) the direct effect of the distant atoms (i.e., the atoms outside the octahedron which are distributed with a trigonal symmetry), or; (ii) the indirect effect of the distant atoms (i.e., the distant atoms distort the octahedron of waters which in turn cause the observed effect), the thermal expansivity and D parameter data for GA&SH, strongly support McGarvey's proposal. Analogous arguments cannot be used to interpret the behaviour of the alums because they are cubic and so the expansivity is isotropic.

Other factors such as the angle of tilt of the water molecules

or the displacement of the chromium ion from the centre of the octahedron of waters may also give a contribution to the D. As shown in Figure 10, the behavior of the D parameter vs temperature is not linear for the RbAℓ and Cs Aℓ alums. The two complexes of GAℓSH behave similarly, having more resemblance to the CsAℓ alum curve. From these curves it can be seen that as the temperature is decreased the slope changes, indicating that possibly more than one mechanism is operative in contributing to the D value, or the expansion and compression of the octahedra are simply non-linear with temperature.

An important aspect investigated by Danilov[1] and supported by the studies reported here is the relationship between the size of the monovalent ion, the size of the trivalent ion, and the value of the D parameter. Danilov[1] found that rubidium gallium alum, which is α-type had a positive D value and that caesium gallium alum which is β-type had a negative D. It was proposed that the sign of the D is perhaps dependant upon the monovalent ion, and hence on the type of alum. In Danilov's work, the trivalent chromium ion, with ionic radius 0.63Å, substituted for a gallium ion, with ionic radius 0.62Å. Since the two ionic radii are similar, the problem of interpretation of the experimental results is simplified because no effect need be attributed to the size of the trivalent ion as is often invoked by others. In the present study, the chromium ion was substituted for an aluminum ion having an ionic radius of 0.51Å, which is about 20% smaller than the gallium ion.

In spite of this significant size difference the D value of the CsAℓ alum was found to be the same sign, negative and nearly the same magnitude as for CsGa alum, while the D value for RbAℓ alum was found to be positive, the same as for the RbGa alum but considerably smaller in magnitude. If size effect was important in causing a distortion of the octahedron then one would expect the D value for RbAℓ alum to be greater than for the case of the RbGa alum. The values of the D's and other parameters for $^{53}Cr^{3+}$ in the crystals being discussed are presented in Table 7.

VI 3 The Quadrupole Term

As previously stated, the D parameter has been related to the electric field gradient V_{zz} according to the relation,

$$D = \frac{3}{7} (\lambda/\Delta E)^2 \langle r^2 \rangle V_{zz} \qquad (5)$$

Thus knowing D, one can calculate V_{zz} which must be known in order to calculate the electric quadrupole moment, Q, of the chromium 53 nucleus as given by

$$Q' = \frac{3eQ\ V_{zz}}{4I(2I - 1)} (1 - \gamma_\infty) \qquad (12)$$

The Q' calculated from this work for RbAℓ alum is of the same order of magnitude and the same sign as found previously for RbGa alum. The same is true for the CsAℓ and CsGa alums. However, in the two types

Table 7

Spin Hamiltonian parameters and related data for some alums and GAℓSH

Parameter	RbAℓ alum	RbGa alum [1]	CsAℓ alum	CsGa alum [1]	GAℓSH(1) [2]	GAℓSH(2) [2]
A	17.3573	17.3722	17.2038	17.2119	17.0774	17.0982
B	17.2738	17.2914	17.4587	17.4754	17.4273	17.4236
(A-B)	0.0835	0.0808	-0.2549	-0.2635	-0.3499	-0.3254
Q'	-0.0215	-0.0164	0.1545	0.1546	0.1682	0.1866
D	348.8	534.2	-715.0	-670.1	-1,155.3	-888.7
V_{zz}	0.8405	1.287	-1.704	-1.597	-2.637	-2.029
Q	-0.0085	-0.0042	-0.030	-0.032	-0.021	-0.031

All in units of 10^{-4} cm^{-1} except Q which is in barns

1. from Reference 16.
2. from Reference 18.

of Rb alums the Q' values are about an order of magnitude smaller than for the two Cs alums. The lack of consistency between the Q' values in the Cs and Rb alums manifests itself in predicting two sets of values for the quadrupole moment , Q, of ^{53}Cr when using equations (5) and (12). Obviously both values cannot be correct and so we must determine from the experimental work where the inconsistency lies.

In the ENDOR work on the gallium alums it was postulated that the result obtained for the CsGa alum was probably the correct one. The basis of the argument was that since the magnitude of the D value changed so little for CsGa alum between the temperatures 300°K and 4.2°K then it is likely that equation (5) could predict the correct value of V_{zz}. For RbGa alum the change in D is large and there is a possibility that a linear relationship might not exist between the spin Hamiltonian parameters and T. This effect is in fact found to be true for the Aℓ alums as shown in figure 10.

The quadrupole moment of ^{53}Cr can be calculated, at 4.2°K, using equation (5) and (12) with the measured values of D and Q'. For CsAℓ alum the value found is Q = -0.030b and for RbAℓ alum it is -0.0085b. The value for the Cs alum is seen to be very close to the value of $|Q| = 0.026b$ predicted by Artman[20] in a theoretical analysis of the transition-metal sesquioxides (Aℓ oxide type lattices). The value for Rb alum is considerably lower than the predicted value. Since the difficulty in the case of the Rb alums is believed to arise

due to the small value of Q' obtained at 4.2°K without a consistently small value of D the following exercise was performed. It was assumed that Q = -0.030b as found in CsAℓ alum. Equation (12), with the $\overline{Q}'$ value measured in RbAℓ alum, was solved for V_{zz}. This gave a value of $V_{zz} = 0.239 \times 10^{-4} cm^{-1}/b$ for RbAℓ alum at 4.2°K. This value of V_{zz} was then put into equation (5) which was solved for D. The calculation predicted a value of $D = 99.2 \times 10^{-4} cm^{-1}$ which is very close to the value of $D = 100 \times 10^{-4} cm^{-1}$ predicted by the high temperature region, straight line part of the curve for RbAℓ alum of figure 10 extended to 4.2°K. Of course the intercept of the extended line is only approximate since only three points are used in plotting the curves of Figure 10. Nevertheless, the curve is believed to be close to reality because it follows the same trend as that for CsAℓ alum and in the two GAℓSH complexes. That is, the lines are straight, down to a point about 60°K above the liquid nitrogen temperature after which they curve to meet the nearly straight lines between 77°K and 4.2°K.

Hence, from the above analysis, it would appear that the crystals behave such that $Q' \propto T$, $V_{zz} \propto T$ and $Q' \propto V_{zz}$, but D is not necessarily proportional to T. The best values of the quadrupole moment of ^{53}Cr can now be obtained by averaging the results found in CsAℓ and CsGa alums and in the two GAℓSH complexes. This is found to be Q = -0.0285b. In the study of ^{53}Cr in $Aℓ_2O_3$ (ruby) Terhune et al.[21] found a value Q = -0.03. Artman and Murphy[22] have previously predicted

the value to be between 0.02 and 0.05b from theoretical considerations of the ruby crystal. With regard to the sign of Q, equation (5) implies that the sign of V_{zz} follows the sign of D. The sign of D has been found experimentally in the ESR and ENDOR work, and so the sign of Q follows from equation (12).

VI 4 The A and B parameters

The anisotropic nature of the hyperfine interaction was not measureable in the alums until ENDOR studies were performed. McGarvey[17] has given the following expressions which describe the A and B parameters

$$A = P\left[\frac{4}{21}(1 - 2a^2 + b^2) - K\right] \qquad (38)$$

$$B = P\left[-\frac{2}{21}(1 - 2a^2 + b^2) - K\right] \qquad (39)$$

Here $P = .40 \times 10^{-4}\,cm^{-1}$ for $^{53}Cr^{3+}$; the first term in the square brackets arises from the electron-nuclear dipole-dipole interaction, while the K represents the contribution due to the Fermi contact term. For a site with octahedral symmetry of the coordinated ligands we have $a^2 = 2/3$; $b^2 = 1/3$ and $1 - 2a^2 + b^2 = 0$, giving A = B from equations (36) and (37). In this case the hyperfine interaction is isotropic and is given by PK. If $a^2 < 2/3$ and $b^2 > 1/3$ then $1 - 2a^2 + b^2$ is positive and A < B. McGarvey shows that the D parameter is negative for

this case and the coordinated octahedron is trigonally compressed. If $a^2 > 3/2$ and $b^2 < 1/3$ then $1 - 2a^2 + b^2$ is negative, giving A > B. This case corresponds to a positive D and a trigonal extension of the octahedron.

The ENDOR results show that the hyperfine interaction is anisotropic with A > B for RbAℓ alum and A < B for CsAℓ alum. This effect is correlated with the fact that D is positive for RbAℓ alum and negative for CsAℓ alum.

VI 5 New Relations between the Parameters

Since the distortion of the octahedron of water molecules surrounding a chromium ion is related to both Q' and the hyperfine parameters it was concluded that it might be instructive to plot Q' vs (A-B) for the alums and GAℓSH, where accurate ENDOR measurements have been made. This plot is shown in figure 13. It is seen that all the points fall close to a straight line. It is also seen that the points for the Rb alums are very close together and the same is true for the Cs alums.

After finding the above linear relationship other plots were made relating all those parameters which were in some way connected to the distortion of the octahedron. This is shown in figure 14. The Q' and (A-B) curves are oriented on this figure consistent with the results of figure 13, i.e. $Q' = A-B = 0.015 \times 10^{-4}\,cm^{-1}$ and $Q' = -(A-B) = 0.05 \times 10^{-4}\,cm^{-1}$

Figure 13. A plot of (A-B) vs Q' for chromium magnetic complexes in alums and GAℓSH at 4.2°K. RbAℓ signifies $RbA\ell(SO_4)_2.12H_2O$, etc., and G(1), G(2) represent the two complexes of GAℓSH.

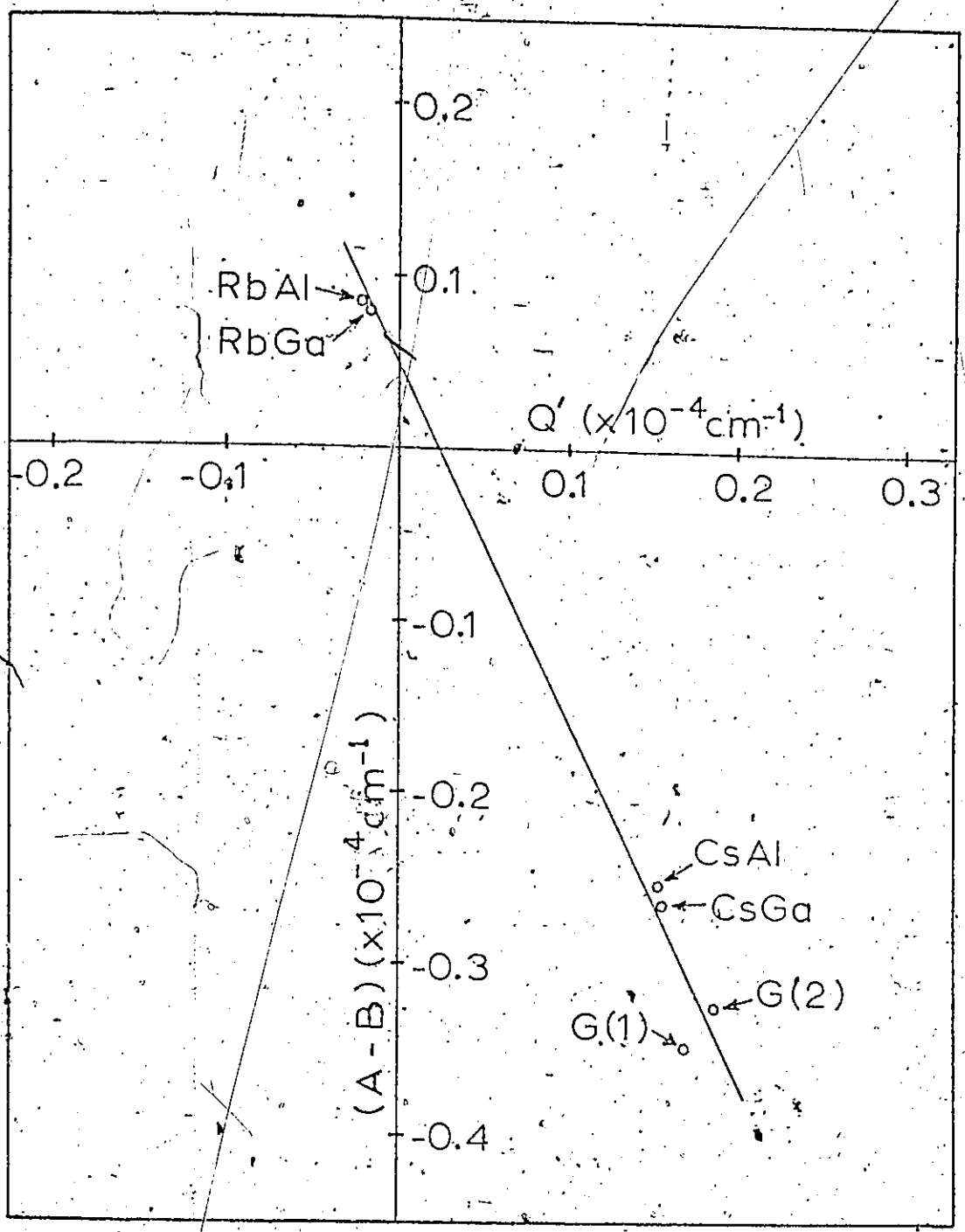
0.2
0.1
RbAl
RbGa
Q' (x10⁻⁴cm⁻¹)
-0.2
-0.1
0.1
0.2
0.3
-0.1
-0.2
-0.3
-0.4
(A-B) (x10⁻⁴cm⁻¹)
CsAl
CsGa
G(2)
G(1)

Figure 14. A plot of A-B, Q' and V_{zz} vs $D_{4.2^oK}$ for the chromium magnetic complexes in alums and GA&SH at 4.2°K. Labeling is as in Figure 13; note the different scales. The V_{zz} points on the left side of the diagram were calculated from equation (5) while the ones on the right side are predicted values calculated from equation (12) assuming a value of Q of -0.0285b.

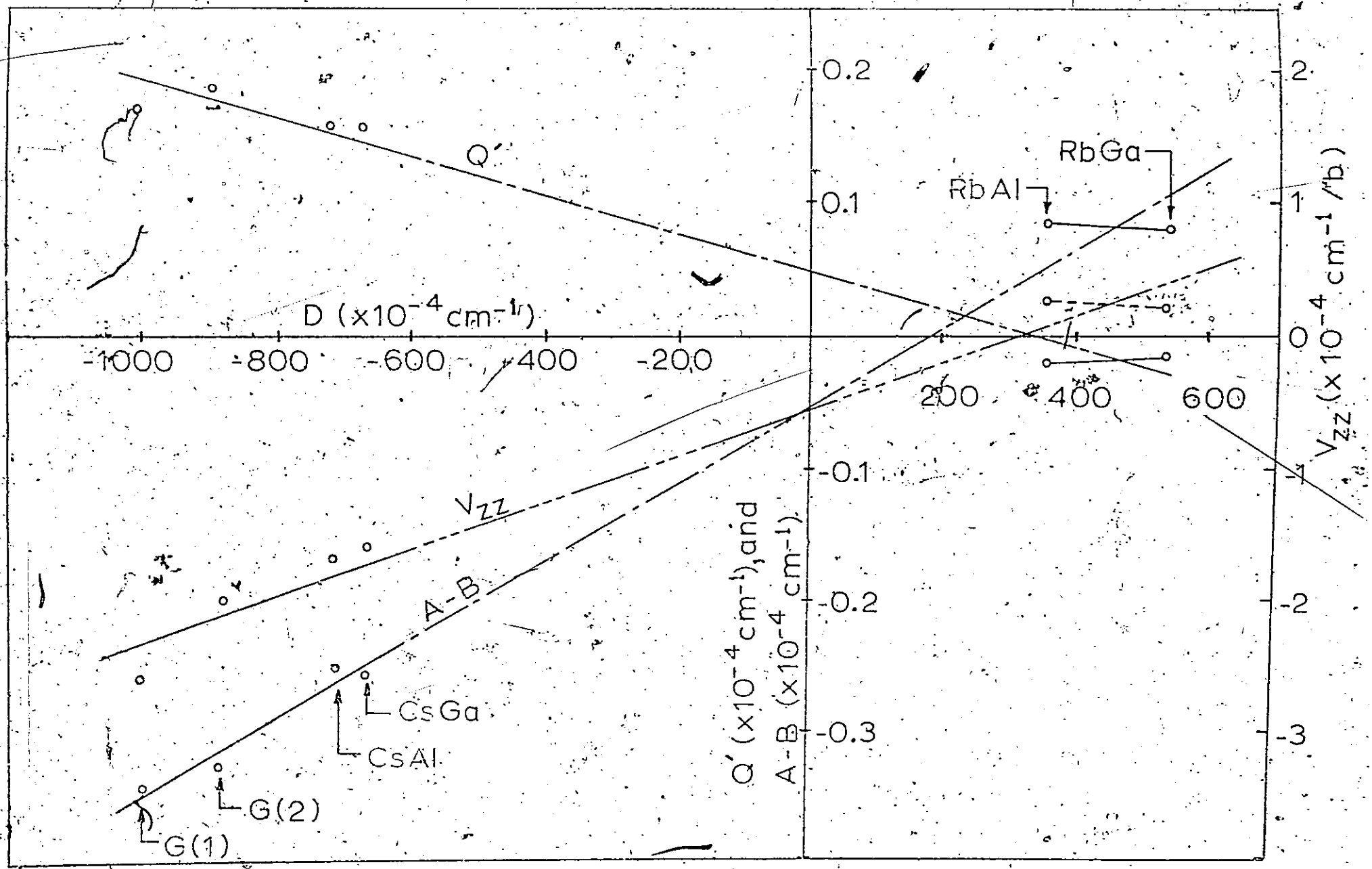
Q'
D (x10^{-4} cm^{-1})
-1000
-800
-600
-400
-200
0.2
0.1
-0.1
-0.2
-0.3
RbGa
RbAl
200
400
600
2
1
0
-2
-3
V_{zz} (x 10^{-4} cm^{-1} /b)
V_{zz}
A-B
CsGa
CsAl
G(2)
G(1)
Q' (x10^{-4} cm^{-1}), and
A-B (x10^{-4} cm^{-1}).

in both figures. The straight lines of figure 13 and 14 fit the experimental points quite well for the negative D values but they are only close to the lines for the positive D.

Using the average value of Q = -0.0285 found for the two Cs alums and GAℓSH it is possible to predict values of V_{zz} to be consistent with the Q' and D values found in the Rb alums. These are found to be 0.2515 and $0.1918 \times 10^{-4} cm^{-1}/b$ for RbAℓ and CsAℓ alum, respectively. A best straight line through all the V_{zz} vs $D_{4.2^oK}$ points can now be drawn, and this is also shown in figure 14. Here again, only a rough fit is obtained for the Rb alums. As described above, the reason for the poor fit of Q' vs D for RbAℓ alum is likely due to the non-linear temperature dependence of D in this alum. It might be instructive to plot the D value, as determined by the intercepts of the curves in Figure 10, as a function of Q' to obtain a better fit with all the points on figure 14. However, it is thought that this exercise can be more profitably done when more experimental points are available.

From these results, particulary those shown in figure 13, we can conclude that it is the monovalent ion which governs the behavior of the alums to the extent that the behavior is described by the spin Hamiltonian parameters, at least for the case of those alums that have been studied so far by the ENDOR technique.

VI 6 The Nuclear g-value

The effective nuclear g-value, g_n' was found to be isotropic in both alums studied. However, unlike the previous work on the gallium alums, slightly different magnitudes of g_n' were found for the two alums. It is not known whether this constitutes a manifestation of some physical effect or is simply a result of an increase in the accuracy of the present measurements or a different method of fitting the parameters. The true nuclear g-value, g_n, is related to g_n' as $g_n = g_n'/(1 + \sigma)$, where σ is the shielding parameter. The value of σ can be calculated from Geshwind's[23] formula

$$\sigma = -5.84 \langle 1/r^3 \rangle_{a.u.} (\Delta g/\lambda) \qquad (40)$$

where Δg is the electronic g-value shift from 2.0023, λ is the spin-orbit coupling parameter of Cr^{3+} in units of cm^{-1}, and $\langle 1/r^3 \rangle$ is the average value of $1/r^3$ for the Cr^{3+} 3d wave function. Using the Cr^{3+} free-ion value of $\lambda = 91\ cm^{-1}$, $\langle 1/r^3 \rangle = 3.959$ a.u., $\Delta g = -0.028$, one finds $\sigma = 0.00744$ which gives a g_n value of -0.3147 for RbAl alum and -0.3117 for CsAl alum. Since the nuclear magnetic moment is $\mu_n = g_n I$, we calculate the magnetic moment of ^{53}Cr to be -0.4721 μ_N and -0.4676 μ_N from the data obtained in the two crystals. These values are close to the Handbook[24] value -0.4735 μ_N obtained from the NMR studies of ^{53}Cr in solution. Danilov and Manoogian[16] found the value to be -0.4640 μ_N for their work on the $^{53}Cr^{3+}$ in the gallium alums.

VI 7 Future Work

In order to better understand the behavior of the alums and the nature of the distortion of the octahedral surroundings of the $^{53}Cr^{3+}$ ion, more studies should be done. It has been demonstrated that equation (5) does not adequately describe the relationship between the D parameter and V_{zz} for the RbAℓ alum and it is probably only approximately true even though it predicts better values for the other crystals. More data is needed to further describe the D vs T relationship for the crystals studied and more crystals must be studied to provide more points for figure 14 before a more comprehensive theory is developed. It would be useful, for example, to study thallium aluminum and thallium gallium alum to provide more information on the effects of the monovalent ion.

APPENDIX I

THE SPIN HAMILTONIAN MATRIX ELEMENTS

Table 8(i) The z-direction diagonal elements.

8(ii) The z-direction off diagonal elements

8(iii) The $\perp$-direction diagonal elements

8(iv) The $\perp$-direction off diagonal elements.

Table 8

SPIN HAMILTONIAN MATRIX ELEMENTS INCLUDING THE HYPERFINE STRUCTURE FOR THE ORIENTATION $H = H_z$.

8(i) Diagonal elements

$< M_I \; M_S \; |H| \; M_S \; M_I >$

$< 3/2 \; 3/2 \; |H| 3/2 \; 3/2 > = (3/2 g_{II} \beta H_z) - 3/2(g'_{nII} \beta_n H_z) + 9/4A + D + Q'$

$< 1/2 \; 3/2 \; |H| 3/2 \; 1/2 > = (\; " \;) - 1/2(\; " \;) + 3/4A + D - Q'$

$< -1/2 \; 3/2 \; |H| 3/2 \; -1/2 > = (\; " \;) + 1/2(\; " \;) - 3/4A + D - Q'$

$< -3/2 \; 3/2 \; |H| 3/2 \; -3/2 > = (\; " \;) + 3/2(\; " \;) - 9/4A + D + Q'$

$< 3/2 \; 1/2 \; |H| 1/2 \; 3/2 > = (1/2 g_{II} \beta H_z) - 3/2(g'_{nII} \beta_n H_z) + 3/4A - D + Q'$

$< 1/2 \; 1/2 \; |H| 1/2 \; 1/2 > = (\; " \;) - 1/2(\; " \;) + 1/4A - D - Q'$

$< -1/2 \; 1/2 \; |H| 1/2 \; -1/2 > = (\; " \;) + 1/2(\; " \;) - 1/4A - D - Q'$

$< -3/2 \; 1/2 \; |H| 1/2 \; -3/2 > = (\; " \;) + 3/2(\; " \;) - 3/4A - D + Q'$

$$\langle 3/2\,-1/2|H|-1/2\;3/2\rangle = (-1/2 g_{II}\beta H_z) - 3/2(g'_{nII}\beta_n H_z) - 3/4A-D+Q'$$

$$\langle 1/2\,-1/2|H|-1/2\;1/2\rangle = (\quad " \quad) - 1/2(\quad " \quad) - 1/4A-D-Q'$$

$$\langle -1/2\,-1/2|H|-1/2\,-1/2\rangle = (\quad " \quad) + 1/2(\quad " \quad) + 1/4A-D-Q'$$

$$\langle -3/2\,-1/2|H|-1/2\,-3/2\rangle = (\quad " \quad) + 3/2(\quad " \quad) + 3/4A-D+Q'$$

$$\langle 3/2\,-3/2|H|-3/2\;3/2\rangle = (-3/2 g_{II}\beta H_z) - 3/2(g'_{nII}\beta_n H_z) - 9/4A+D+Q'$$

$$\langle 1/2\,-3/2|H|-3/2\;1/2\rangle = (\quad " \quad) - 1/2(\quad " \quad) - 3/4A+D-Q'$$

$$\langle -1/2\,-3/2|H|-3/2\,-1/2\rangle = (\quad " \quad) + 1/2(\quad " \quad) + 3/4A+D-Q'$$

$$\langle -3/2\,-3/2|H|-3/2\,-3/2\rangle = (\quad " \quad) + 3/2(\quad " \quad) + 9/4A+D+Q'$$

8 (ii) Off diagonal elements

$$\langle \pm 3/2 \pm 1/2| \;|\pm 1/2 \pm 1/3\rangle = (3/2\ B)$$

$$\langle \mp 1/2 \pm 1/2| \;|\mp 3/2 \pm 3/2\rangle = "$$

$$\langle \mp 3/2 \mp 1/2|H|+1/2 \pm 1/2\rangle = "$$

$$\langle +1/2 \mp 3/2|H|+1/2 \mp 3/2\rangle = "$$

$\langle M_I\ M_S\ |H|\ M_S\ M_I \rangle$

$\langle \pm 1/2 \pm 1/2 |H| \pm 3/2 \mp 1/2 \rangle = (\sqrt{3}\ B)$

$\langle \pm 3/2 \mp 1/2 |H| \pm 1/2 \pm 1/2 \rangle = \quad "$

$\langle \mp 1/2 \mp 1/2 |H| \pm 1/2 \mp 3/2 \rangle = \quad "$

$\langle \pm 1/2 \mp 3/2 |H| \mp 1/2 \mp 1/2 \rangle = \quad "$

$\langle \pm 1/2 \mp 1/2 |H| \pm 1/2 \mp 1/2 \rangle = 2\ B$

All other elements in this manifold are zero.

SPIN HAMILTONIAN MATRIX ELEMENTS INCLUDING THE HYPERFINE STRUCTURE WHEN THE MAGNETIC FIELD IS PERPENDICULAR TO THE Z AXIS.

8(iii) Diagonal elements.

$< M_S \; M_S \; |H| \; M_S \; M_I >$

$< 3/2 \; 3/2 \; |H| 3/2 \; 3/2> = (3/2 g_\perp \beta H_\perp) - 3/2 (g_{n\perp} \beta_n H_\perp) + 9/4 \; B \; -1/2D-1/2Q'$

$< 1/2 \; 3/2 \; |H| 3/2 \; 1/2> = (\; " \;) - 1/2 (\; " \;) + 3/4 \; B \; -1/2D+1/2Q'$

$<-1/2 \; 3/2 \; |H| 3/2 -1/2> = (\; " \;) + 1/2 (\; " \;) - 3/4 \; B \; -1/2D+1/2Q'$

$<-3/2 \; 3/2 \; |H| 3/2 -3/2> = (\; " \;) + 3/2 (\; " \;) - 9/4 \; B \; -1/2D-1/2Q'$

$< 3/2 \; 1/2 \; |H| 1/2 \; 3/2> = (1/2 g_\perp \beta H_\perp) - 3/2 (g_{n\perp} \beta_n H_\perp) + 3/4 \; B \; +1/2D-1/2Q'$

$< 1/2 \; 1/2 \; |H| 1/2 \; 1/2> = (\; " \;) - 1/2 (\; " \;) + 1/4 \; B \; +1/2D+1/2Q'$

$<-1/2 \; 1/2 \; |H| 1/2 -1/2> = (\; " \;) + 1/2 (\; " \;) + 1/4 \; B \; +1/2D+1/2Q'$

$<-3/2 \; 1/2 \; |H| 1/2 -3/2> = (\; " \;) + 3/2 (\; " \;) - 3/4 \; B \; +1/2D-1/2Q'$

$$\langle 3/2\text{-}1/2 \mid H \mid -1/2\ 3/2\rangle = (-1/2 g_{\perp}\beta H_{\perp}) - 3/2(g'_{n\perp}\beta_n H_{\perp}) - 3/4\ B + 1/2D - 1/2Q'$$

$$\langle 1/2\text{-}1/2 \mid H \mid -1/2\ 1/2\rangle = (\ \ " \ \ ) - 1/2(\ \ " \ \ ) - 1/4\ B + 1/2D + 1/2Q'$$

$$\langle -1/2\text{-}1/2 \mid H \mid -1/2\text{-}1/2\rangle = (\ \ " \ \ ) + 1/2(\ \ " \ \ ) + 1/4\ B + 1/2D + 1/2Q'$$

$$\langle -3/2\text{-}1/2 \mid H \mid -1/2\text{-}3/2\rangle = (\ \ " \ \ ) + 3/2(\ \ " \ \ ) + 3/4\ B + 1/2D - 1/2Q'$$

$$\langle 3/2\text{-}3/2 \mid H \mid -3/2\ 3/2\rangle = (-3/2 g_{\perp}\beta H_{\perp}) - 3/2(g'_{n\perp}\beta_n H_{\perp}) - 9/4\ B - 1/2D - 1/2Q'$$

$$\langle 1/2\text{-}3/2 \mid H \mid -3/2\ 1/2\rangle = (\ \ " \ \ ) - 1/2(\ \ " \ \ ) - 3/4\ B - 1/2D + 1/2Q'$$

$$\langle -1/2\text{-}3/2 \mid H \mid -3/2\text{-}1/2\rangle = (\ \ " \ \ ) + 1/2(\ \ " \ \ ) + 3/4\ B - 1/2\ D + 1/2Q'$$

$$\langle -3/2\text{-}3/2 \mid H \mid -3/2\text{-}3/2\rangle = (\ \ " \ \ ) + 3/2(\ \ " \ \ ) + 9/4\ B - 1/2\ D - 1/2Q'$$

8(iv) Off-diagonal elements

$\langle M_I \; M_S | H | \; M_S \; M_I \rangle$

$\langle \mp 1/2 \; 3/2 | H | \; 3/2 \mp 3/2 \rangle = (\sqrt{3}/2)\, Q'$

$\langle \mp 3/2 \; 3/2 | H | \; 3/2 \pm 1/2 \rangle = \;"$

$\langle \mp 1/2 \; 1/2 | H | \; 1/2 \pm 3/2 \rangle = \;"$

$\langle \mp 3/2 \; 1/2 | H | \; 1/2 \pm 1/2 \rangle = \;"$

$\langle \mp 1/2 - 1/2 | H | -1/2 \pm 3/2 \rangle = \;"$

$\langle \mp 3/2 - 1/2 | H | -1/2 \pm 1/2 \rangle = \;"$

$\langle \mp 1/2 - 3/2 | H | -3/2 \pm 3/2 \rangle = \;"$

$\langle \mp 3/2 - 3/2 | H | -3/2 \pm 1/2 \rangle = \;"$

$\langle \pm 3/2 \pm 1/2 | H | \pm 3/2 \pm 1/2 \rangle = (3/2)\,V$

$\langle \mp 1/2 \pm 1/2 | H | \pm 3/2 \mp 3/2 \rangle = \;"$

$\langle \pm 3/2 \mp 3/2 | H | \mp 1/2 \pm 1/2 \rangle = \;"$

$\langle \mp 1/2 \mp 3/2 | H | \mp 1/2 \mp 3/2 \rangle = \;"$

$\langle \pm 1/2 \pm 1/2 | H | \pm 3/2 \mp 1/2 \rangle = \sqrt{3}\, A$

$\langle \pm 3/2 \mp 1/2 | H | \pm 1/2 \pm 1/2 \rangle =$ "

$\langle \mp 1/2 \mp 1/2 | H | \pm 1/2 \mp 3/2 \rangle =$ "

$\langle \pm 1/2 \mp 3/2 | H | \mp 1/2 \mp 1/2 \rangle =$ "

$\langle \pm 1/2 \mp 1/2 | H | \pm 1/2 \mp 1/2 \rangle = 2\, A$

$\langle \pm 3/2 \mp 1/2 | H | \pm 3/2 \pm 3/2 \rangle = (\sqrt{3}/2)\, D$

$\langle \pm 1/2 \mp 1/2 | H | \pm 3/2 \mp 1/2 \rangle =$ "

$\langle \mp 1/2 \mp 1/2 | H | \pm 3/2 \mp 1/2 \rangle =$ "

$\langle \mp 3/2 \mp 1/2 | H | \pm 3/2 \mp 3/2 \rangle =$ "

$\langle \pm 3/2 \mp 3/2 | H | \pm 1/2 \pm 3/2 \rangle =$ "

$\langle \pm 1/2 \mp 3/2 | H | \pm 1/2 \pm 1/2 \rangle =$ "

$\langle \mp 1/2 \mp 3/2 | H | \pm 1/2 \mp 1/2 \rangle =$ "

$\langle \mp 3/2 \mp 3/2 | H | \pm 1/2 \mp 3/2 \rangle =$ "

All other matrix elements in this manifold are zero.

APPENDIX 2

The listing and an example of the output of the computer program used for the z-direction calculations. The $\perp$-direction program was the same except for the matrix elements.

```
C*************************************************************************
C
C
C                         Z   DIRECTION
C
C
C*************************************************************************
C
C
C     THIS PROGRAM DIAGONALIZES A (16,16) MATRIX 'A' WHICH REPRESENTS
C     THE ENERGY STATES OF A CHROMIUM 53 ATOM IN A TRIGONALLY DISTORTED
C     CUBIC ELECTRIC FIELD WITH THE MAGNETIC FIELD ALONG THE Z-AXIS OF
C     THE CRYSTAL. THE VALUES OF THE HAMILTONIAN PARAMETERS ARE READ
C     IN, THE SUBROUTINE EIGEN DIAGONALIZES THE MATRIX AND ORDERS THE
C     EIGENVALUES IN ORDER OF DECREASING ENERGY . THESE ARE THEN
C     SUBTRACTED TO GIVE THE ENERGY IN MEGACYCLES OF TRANSITIONS
C     OCCURING BETWEEN THESE LEVELS , ALL FOR THE PARTICULAR HAMILTONIAN
C     PARAMETERS GIVEN. A COMPARISON IS MADE BETWEEN THE CALCULATED AND MEASURED
C     MEASURED VALUES.
C     FACILITY ALSO EXISTS FOR THE AUTOMATIC VARIATION OF THE
C     HAMILTONIAN PARAMETERS EXCEPT G. THE VALUES OF HTOMC AND BNONBG
C     CONTAIN THE G AND THESE VALUES MUST BE CHANGED MANUALLY WHEN
C     THE VALUE OF THE G-VALUE IS CHANGED.
C
C
C     THE EXPLANATION OF A'S DIMENSION IS GIVEN IN MY NOTES PAGES 54,55
C
C     MV IS A CODE FOR OUTPUT
C      0 SIGNIFIES FINDING BOTH EIGENVECTORS AND EIGENVALUES
C      1 SIGNIFIES FINDING ONLY THE EIGENVALUES.
C
C      N IS THE ORDER OF THE A AND R MATRICIES
C
C     HPLANK = 6.6262
C     BOHR = 9.2741
C     NUCLEAR MAGNETON = 5.0509
C
C     USE OF THESE CONVERSION FACTORS ENABLES EASY ALTERATION OF G-VALUE
C
C     HTOMC = (G*BOHR)/HPLANK
C     BNONBG = B-NUCLEAR/(B-ELECTRONIC*G)
C
C
```

```
      C     TEXT IS THE TITLE OF THE OUTPUT
      C
      C     HA(K) ARE THE SPECIFIC FIELD VALUES FOR WHICH
      C      MEASUREMENTS WERE TAKEN.
      C
      C     AMEASR(K,J) ARE THE MEASURED TRANSITION FREQUENCIES
      C
      C     THE 'MOOG' LOOP INCREMENTS THE HAMILTONIAN PARAMETER VALUE
      C     SEE LAST STATEMENT BEFORE RETURN,#88,FOR EXACT CHANGE MADE.
      C
      C
0001        DOUBLE PRECISION S(16),HA(10),DEL(12),G,AMC,BMC,HTOMC,CPRIME,AHYP
0002        DOUBLE PRECISION DIFF(8,12),AMEASR(8,12),D,GNPRIM,QMC,BNONBG,BHYP
0003        DIMENSION TEXT(20),A(136)
0004        MV=1
0005        N=16
0006        HTOMC = 2.76549
0007        BNONBG = .275634D-3
0008        READ (1,101) (TEXT(J),J=1,18)
0009  101   FORMAT (20A4)
0010        READ (1,2) (D,G,GNPRIM,AMC,QMC,BMC)
0011      2 FORMAT (3(F12.6),3(F12.8))
0012        READ (1,33) (HA(M) , M = 1,8 )
0013  33    FORMAT ( 8F8.5 )
      C
      C
0014        DO 99 K = 1,8
0015        DO 98 J= 1,12
0016  98    AMEASR(K,J) = 0.0
0017  99    CONTINUE
      C
0018        AMEASR(1,1) = 77.960
0019        AMEASR(1,2) = 78.517
0020        AMEASR(2,1) = 77.969
0021        AMEASR(2,2) = 78.522
0022        AMEASR(2,3) = 79.084
0023        AMEASR(3,1) = 77.973
0024        AMEASR(3,2) = 78.532
0025        AMEASR(3,3) = 79.092
0026        AMEASR(4,1) = 77.995
0027        AMEASR(4,2) = 78.542
0028        AMEASR(4,3) = 79.093
0029        AMEASR(5,11) = 77.328
```

```
0030            AMEASR(5,12) = 77.036
0031            AMEASR(6,10) = 77.640
0032            AMEASR(6,11) = 77.338
0033            AMEASR(6,12) = 77.033
0034            AMEASR(7,10) = 77.643
0035            AMEASR(7,11) = 77.333
0036            AMEASR(7,12) = 77.024
0037            AMEASR(8,10) = 77.635
0038            AMEASR(8,11) = 77.324
0039            AMEASR(8,12) = 77.022
                C
                C
                C
0040            HTOMC = HTOMC*10**3
                C
                C
0041            DO 88 MOOG = 1,10
0042            WRITE (3,102)(TEXT(J),J=1,18)
0043          102 FORMAT ('1',10X,20A4,//)
0044            WRITE (3,103)(D,G,GNPRIM,AMC,QMC,BMC)
0045          103 FORMAT (10X,'D = ',F12.6,'  KILOGAUSS',/,10X,'G = ',F12.6,' ELECTRONIC
                1ONIC G',/,10X,'GN = ',F12.6,'  NUCLEAR G',/,10X,'A = ',F12.8,'    MC
                2 MC    ',/,10X,'Q = ',F12.8,'*10-4 CM-1 ',/,10X,'B = ',F12.8,'
                3'    MC      ',////)
0046            WRITE (3,100)
0047          100 FORMAT(63X, '  TRANSITION  FREQUENCIES - ' ,///)
0048            WRITE(3,25)
0049          25  FORMAT(50X, ' CALCULATED        MEASURED      DIFFERENCE ' //)
                C
                C   CONVERTING TO KILOGAUSS FOR CALCULATION
                C
0050            AHYP = (AMC /2.7652)*10E-4
0051            BHYP = (BMC /2.7652)*10E-4
0052            QPRIME = QMC   *.1070446E-2
                C
                C
                C
                C   THE 'K' LOOP CHANGES THE FIELD VALUE.
                C
0053            DO 3 K = 1,8
0054            DO 14 I=1,136
0055          14 A(I)=0.0
0056            A(12)=1.5*BHYP
```

```
0057            A(18)=SQRT(3.)*BHYP
0058            A(25)=1.5*BHYP
0059            A(42)=SQRT(3.)*BHYP
0060            A(52)=2.0*BHYP
0061            A(63)=SQRT(3.)*BHYP
0062            A(88)=1.5*BHYP
0063            A(102)=SQRT(3.)*BHYP
0064            A(117)=1.5*BHYP
0065            A(1)=1.5*HA(K)-(1.5*GNPRIM *  BNONBG  *HA(K))+D+2.25*AHYP+QPRIME
0066            A(3)=1.5*HA(K)-(.5*GNPRIM *  BNONBG  *HA(K))+D+.75*AHYP-QPRIME
0067            A(6)=1.5*HA(K)+(.5*GNPRIM *  BNONBG  *HA(K))+D-.75*AHYP-QPRIME
0068            A(10)=1.5*HA(K)+(1.5*GNPRIM *  BNONBG  *HA(K))+D-2.25*AHYP+QPRIME
0069            A(15)=.5*HA(K)-(1.5*GNPRIM *  BNONBG  *HA(K))-D+.75*AHYP+QPRIME
0070            A(21)=.5*HA(K)-.5*GNPRIM*  BNONBG  *HA(K)-D+.25*AHYP-QPRIME
0071            A(28)=.5*HA(K)+.5*GNPRIM *  BNONBG  *HA(K)-D-.25*AHYP-QPRIME
0072            A(36)=.5*HA(K)+1.5*GNPRIM *  BNONBG  *HA(K)-D-.75*AHYP+QPRIME
0073            A(45)=-.5*HA(K)-1.5*GNPRIM *  BNONBG  *HA(K)-D-.75*AHYP+QPRIME
0074            A(55)=-.5*HA(K)-.5*GNPRIM *  BNONBG  *HA(K)-D-.25*AHYP-QPRIME
0075            A(66)=-.5*HA(K)+.5*GNPRIM *  BNONBG  *HA(K)-D+.25*AHYP-QPRIME
0076            A(78)=-.5*HA(K)+1.5*GNPRIM *  BNONBG  *HA(K)-D+.75*AHYP+QPRIME
0077            A(91)= -1.5*HA(K)-1.5*GNPRIM *  BNONBG  *HA(K)+D-2.25*AHYP+QPRIME
0078            A(105)=-1.5*HA(K)-.5*GNPRIM *  BNONBG  *HA(K)+D-.75*AHYP-QPRIME
0079            A(120)=-1.5*HA(K)+.5*GNPRIM *  BNONBG  *HA(K)+D+.75*AHYP-QPRIME
0080            A(136)=-1.5*HA(K)+1.5*GNPRIM *  BNONBG  *HA(K)+D+2.25*AHYP+QPRIME
                C
                C
0081            CALL EIGEN (A,R,N,MV)
                C
                C
0082            DO 270 I=1,16
0083            L=I+(I*I-I)/2
0084        270 S(I)=A(L)
                C
                C
0085            DEL(1)=(S(1)-S(2))*HTOMC
0086            DEL(2)=(S(2)-S(3))*HTOMC
0087            DEL(3)=(S(3)-S(4))*HTOMC
0088            DEL(4)=(S(5)-S(6))*HTOMC
0089            DEL(5)=(S(6)-S(7))*HTOMC
0090            DEL(6)=(S(7)-S(8))*HTOMC
0091            DEL(7)=(S(9)-S(10))*HTOMC
0092            DEL(8)=(S(10)-S(11))*HTOMC
0093            DEL(9)=(S(11)-S(12))*HTOMC
```

```
0094                DEL(10)=(S(13)-S(14))*HTOMC
0095                DEL(11)=(S(14)-S(15))*HTOMC
0096                DEL(12)=(S(15)-S(16))*HTOMC
                C
                C
0097                DO 78 J = 1,12
0098           78   DIFF(K,J) = DEL(J) - AMEASR (K,J)
                C
                C
0099                DO 2001 J = 1,12
0100                IF(AMEASR(K,J).EQ.0.0) GO TO 2001
0101                IF(J.EQ.11.OR.J.EQ.2) GO TO 2002
0102                WRITE (3,180) HA(K) ,(DEL(J),AMEASR (K,J),DIFF(K,J))
0103           180  FORMAT(25X,F8.5, ' KILOGAUSS ' ,5X,12(3(F10.6, 'MC ' ,5X),/49X))
0104                GO TO 2001
0105           2002 WRITE (3,181) HA(K) ,(DEL(J),AMEASR (K,J),DIFF(K,J))
0106           181  FORMAT(25X,F8.5, ' KILOGAUSS ' ,5X,12(3(F10.6, 'MCC' ,5X),/49X))
0107           2001 CONTINUE
0108           3    WRITE(3,3000)
0109           3000 FORMAT(//)
0110                WRITE (3,190)
0111           190  FORMAT(10X, ' ************************************************
                    1********************* ' ,//, ' ********************************
                    2************************************************** ' )
0112                WRITE(3,191)
0113           191  FORMAT('1')
                C
                C
0114           88   AMC = AMC + .0005
                C
                C
0115                RETURN
0116                END
```

C = 0.378470 KILOGAUSS
G = 1.975900 ELECTRONIC G
GN = -0.317000 NUCLEAR G
A = 52.07200000 MC
Q = -0.0215000C*10-4 CM-1
B = 51.82150000 MC

TRANSITION FREQUENCIES

	CALCULATED	MEASURED	DIFFERENCE
2.58113 KILOGAUSS	77.963483MC	77.959991MC	0.003492MC
2.58113 KILOGAUSS	78.514695MCC	78.516998MCC	-0.002303MCC
2.60403 KILOGAUSS	77.971395MC	77.968994MC	0.002401MC
2.60403 KILOGAUSS	78.525244MCC	78.521988MCC	0.003257MCC
2.60403 KILOGAUSS	79.087006MC	79.084000MC	0.003006MC
2.62238 KILOGAUSS	77.979308MC	77.972992MC	0.006316MC
2.62238 KILOGAUSS	78.530519MCC	78.531998MCC	-0.001478MCC
2.62238 KILOGAUSS	79.092280MC	79.091995MC	0.000285MC
2.64131 KILOGAUSS	77.989857MC	77.994995MC	-0.005138MC
2.64131 KILOGAUSS	78.535794MCC	78.541992MCC	-0.006198MCC
2.64131 KILOGAUSS	79.092280MC	79.092987MC	-0.000707MC

4.09246 KILOGAUSS	77.341062MCC	77.327988MCC	0.013075MCC
4.09246 KILOGAUSS	77.035127MC	77.035995MC	-0.000869MC
4.11228 KILOGAUSS	77.641723MC	77.639999MC	0.001724MC
4.11228 KILOGAUSS	77.335788MCC	77.337997MCC	-0.002210MCC
4.11228 KILOGAUSS	77.029852MC	77.032990MC	-0.003137MC
4.13443 KILOGAUSS	77.633811MC	77.642990MC	-0.009179MC
4.13443 KILOGAUSS	77.327876MCC	77.332993MCC	-0.005117MCC
4.13443 KILOGAUSS	77.027215MC	77.023987MC	0.003228MC
4.15775 KILOGAUSS	77.625899MC	77.634995MC	-0.009095MC
4.15775 KILOGAUSS	77.319963MCC	77.323990MCC	-0.004026MCC
4.15775 KILOGAUSS	77.019303MC	77.021988MC	-0.002685MC

APPENDIX 3

The 25 MHz transitions for $^{53}Cr^{3+}$ in CsAℓ and RbAℓ alum.

Note: none of these are harmonics of 75 MHz lines.

Table 9

The 25 MHz lines for Caesium Alum

Z-DIRECTION		⊥-DIRECTION	
FIELD (kG)	ENDOR FREQUENCIES (MHz)	FIELD (kG)	ENDOR FREQUENCIES (MHz)
1.79346	25.545	2.59021	--
		2.60946	--
1.81171	24.552	2.62826	24.716
	26.093		25.935
		2.64770	24.530
1.82998	26.087		24.757
1.84759	--	4.10948	25.083
			25.379
			25.538
4.89620	--	4.12792	25.136
4.91499	24.908		25.532
4.93401	24.895	4.14577	24.654
	25.622		25.103
			25.225
4.95302	--	4.16468	24.652
			25.300

Table 10

The 25 MHz lines for Rubidium Alum

Z-DIRECTION		⊥-DIRECTION	
FIELD (kG)	ENDOR FREQUENCIES (MHz)	FIELD (kG)	ENDOR FREQUENCIES (MHz)
2.58113	25.566	2.96400	25.125
2.60403	25.594		25.387
2.62238	25.583	2.98277	25.126
	26.506		25.389
2.64131	26.516	3.00048	25.136
			25.389
4.09246	26.093	3.02213	25.404
	26.310		25.661
4.11228	26.173		
	26.395		
4.13443	26.263	3.71304	25.023
	26.485	3.73190	25.018
4.15775	26.089		25.239
	26.358	3.75022	25.091
	26.577		25.234
			25.465
		3.76974	25.015
			25.224
			25.459

List of References

1. Danilov, A. G., Ph.D. Thesis, University of Ottawa, (1971).
2. Vegard, Schjelderup, Annalen d. Physik, LIV, p. 146, (1917).
3. Wyckoff, Amer. Journ. of Sci. V, p. 209 (1923).
4. Lipson, H., and Beevers, C. A., Proc. Roy. Soc. A, vol. 148 (1934).
5. Lipson, H., Proc. Roy. Soc. vol. 1511 (1935).
6. Cromer, Kay and Larsen, Acta. Cryst. 21, p. 383, (1966).
7. Pryce, M.H.L., Proc. Roy. Soc., A63, 25 (1950).
8. Abragam, A., Pryce, M.H.L., Proc. Roy. Soc., (London), A205, 135, (1951).
9. O'Reilly, D. E., and Tsang, T., Phys. Rev. 157, 417 (1967).
10. Moser, C. M., Hyperfine Interactions, p. 95 (Academic Press, New York) (1967).
11. Zaviosky, E., Fiz. Zh. 9, 211, 245, (1945).
12. Van Vleck, J. H., Phys. Rev., 57, 426 (1940).
13. Feher, G., Phys. Rev. 103, 500 (1956).
14. Feher, G., Gere, E. A., Phys. Rev. 103, 834, (1956).
15. Danilov, A., and Manoogian, A. Phys. Rev. B6, 4097, (1972).
16. Danilov, A., and Manoogian, A., Phys. Rev. B6, 4103, (1972).
17. McGarvey, B. R., J. Chem. Phys. 40, 809, (1964).
18. Manoogian, A., and Leclerc, A., to be published.

19. Haussuhl, S., and Trost, F., Z. Naturforsch, 14a, 437, (1959).

20. Artman, J. O., Phys. Rev. 143, 541, (1966).

21. Terhune, R. W., Lambe, J., Kikuchi, C., Baker, J., Phys. Rev. 123, 1265, (1961).

22. Artman, J. O., Murphy, J. C., Phys. Rev. 135, A1622, (1964).

23. Geschwind, S., Hyperfine Interactions, edited by A. J. Freeman and R. B. Frankel (Academic Press, New York) p. 243, (1967).

24. Handbook of Chemistry and Physics, 1965, (The Chemical Rubber Company, Cleveland, Ohio).

Post Oral Discussion

The curve between the room and nitrogen temperature points for the RbAℓ alum of Figure 10 was originally drawn after studying the shape of the D vs T curves of certain GAℓSH crystals. It was suggested that other curves could be equally justifiably drawn on the basis of what was known and consequently any conclusion based on extrapolation of this curve was of doubtful validity. Subsequent to the writing of this thesis however, the D parameter for the RbAℓ alum was measured at the carbon dioxide sublimation point and was found to lie exactly on the previously drawn curve, removing any doubt about the conclusions made. The coordinates of this point, which is indicated on Figure 10 are $D = 474 \times 10^{-4} cm^{-1}$, $T = 195^{o}K$.